Revised MS# 201103016

07-12-2011

FAK Is Required for Assembly of Podosome Rosettes

Yi-Ru Pan[1], Chien-Lin Chen[1], and Hong-Chen Chen[1,2,3,4]*

[1]Department of Life Sciences, National Chung Hsing University, Taichung 402, Taiwan; [2]Graduate Institute of Biomedical Sciences, National Chung Hsing University, Taichung 402, Taiwan; [3]Infectious Disease and Signaling Research Center, National Cheng Kung University, Tainan 701, Taiwan; [4]Department of Nutrition, China Medical University, Taichung 404, Taiwan

*Correspondence to Hong-Chen Chen, PhD

E-mail: hcchen@nchu.edu.tw

Phone: 886-4-22854922

Fax: 886-4-22853469

Characters count (excluding Methods and References): 39586

Running Title: FAK is required for podosome rosette assembly

Keywords: FAK, podosome, invadopodia, Cas, Rho, vimentin

Abstract

Podosomes are dynamic, actin-enriched membrane structures that play an important role in invasive cell motility and extracellular matrix degradation. They are often found to assemble into large rosette-like structures in highly invasive cells. However, the mechanism of this assembly remains obscure. In this study, we identified focal adhesion kinase (FAK) as a key molecule necessary for assembly. Moreover, phosphorylation of p130Cas and suppression of Rho signaling by FAK were found to be important for FAK to induce the assembly of podosome rosettes. Finally, we found that suppression of vimentin intermediate filaments by FAK facilitates the assembly of podosome rosettes. Collectively, our results strongly suggest a link between FAK, podosome rosettes, and tumor invasion and unveil a negative role for Rho signaling and vimentin filaments in podosome rosette assembly.

Introduction

Podosomes are dynamic, actin-enriched membrane structures that represent protrusions of the ventral plasma membrane and have an important role in invasive cell motility and extracellular matrix (ECM) degradation (Linder, 2007). Following the discovery of podosomes in fibroblasts transformed by the Rous sarcoma virus (Chen et al., 1985), similar structures have also been found in several types of normal cells, including osteoclasts, macrophages, dendritic cells, endothelial cells, and vascular smooth muscle cells (Linder and Aepfelbacher, 2003). Many invasive cancer cells display structures similar to podosomes, called invadopodia, that represent the major sites of ECM degradation in these cells. The current convention is to use the term podosome for the structures found in normal cells and Src-transformed cells and to call the structures found in invasive cancer cells invadopodia (Gimona et al., 2008).

Podosomes are dot-shaped structures with a diameter of 0.5-1 μm and a height of 0.2-5 μm, composed of a core of F-actin and actin regulators, such as cortactin and the Arp2/3 complex, surrounded by a ring structure containing integrins, scaffolding proteins, and kinases (Linder and Aepfelbacher, 2003). They are found either isolated both in macrophages and dendritic cells or arranged into superstructures in osteoclasts and other

types of cells. In Src-transformed fibroblasts, podosomes are often organized into large rosette-shaped structures with a diameter of 5-20 μm. Such podosome rosettes can also be found in osteoclasts (Destaing et al., 2003), endothelial cells (Tatin et al., 2006), and some highly invasive cancer cells (Kocher et al., 2009). In particular, osteoclasts seeded on glass develop podosomes that are first grouped into clusters, which assemble into small podosome rings (or rosettes) and eventually into a large belt-like structure at the cell periphery (Destaing et al., 2003). When seeded on bone or a bone-like substrate, osteoclasts develop a large and dense F-actin ring, called the sealing zone, where osteoclasts secrete protons and proteases to dissolve and degrade the mineralized matrix (Luxenburg et al., 2007). Therefore, podosomes can serve as the structural unit for superstructures such as podosome rosettes or belts. However, the mechanism of the organization of podosomes into such superstructures remains obscure.

Focal adhesion kinase (FAK), a 125-kDa non-receptor tyrosine kinase localized in focal adhesions, is known for its pivotal role in the control of a variety of cell functions (McLean et al., 2005). FAK was originally identified as a substrate of Src and subsequently found to be activated upon cell adhesion to ECM proteins (Guan and Shalloway, 1992) as well as by some growth factors (Sieg et al., 2000; Chen and Chen, 2006). Y397 is the major site of FAK autophosphorylation, which creates a high-affinity binding site for the

Src-homology (SH) 2 domain of several proteins including the Src family kinases (Schaller et al., 1994). Activated Src phosphorylates FAK on multiple sites including Y576 and Y577, both of which are located in the activation loop within the kinase domain (Calalb et al., 1995). The ensuing phosphorylation of FAK on Y576 and Y577 is required for the full enzymatic activity of FAK. Fibroblasts derived from FAK-null ($FAK^{-/-}$) mouse embryos are more rounded and poorly-spread than their wild-type counterparts (Ilic et al., 1995). They show an overabundance of focal adhesions, enriched cortical actin filaments at the cell periphery, and a decreased migration rate. It has been shown that an increase in peripheral adhesions results from an inhibition of turnover in $FAK^{-/-}$ cells, which may be attributed to constitutive activation of RhoA and Rho-associated kinase (ROCK) (Ren et al., 2000; Chen et al, 2002).

Increased expression and tyrosine phosphorylation of FAK have been correlated with the progression to an invasive cell phenotype (Schlaepfer et al., 2004). Given its close relationship with integrins, focal adhesion proteins, and actin regulators, it is generally believed that FAK plays an important role in podosomes/invadopodia. However, some recent studies do not appear to support this assumption (Vitale et al., 2008; Chan et al., 2009), claiming that while FAK is important for cell invasion, it is not required for the formation of invadopodia in cancer cells. In this study, we demonstrate that while FAK is

dispensable for dot-shaped podosomes, it is required for the assembly of podosome rosettes. Additionally, our results show that the induction of podosome rosettes by FAK promotes matrix degradation and cell invasion, supporting a role of FAK in malignant tumor progression. We propose that FAK may regulate podosome rosettes through its effect on p130Cas phosphorylation, Rho signaling, and vimentin intermediate filaments.

Results

FAK, but not PYK2, is crucial for the formation of podosome rosettes in fibroblasts, endothelial cells, and carcinoma cells

We first examined if FAK plays a role in the formation of podosome rosettes in Src-transformed fibroblasts. Depletion of FAK, but not the other FAK family member PYK2, significantly suppressed podosome rosette formation and Matrigel invasion in Src-transformed mouse embryo fibroblasts (MEFs) (Fig. 1, A-C; Fig. S1) and Src-transformed NIH3T3 cells (Fig. S2). In human umbilical vein endothelial cells (HUVECs), PYK2 was hardly detected (Fig. 1 D). Knockdown of FAK completely suppressed phorbol-12-myristate-13-acetate (PMA)-induced formation of podosome rosettes in HUVECs (Fig. 1 E). In lung carcinoma CL1-5 cells, depletion of FAK, but not PYK2, led to a decreased formation of rosette-like structures in the cells (Fig. 1, F and G). These structures are truly podosome rosettes, because they are exclusively found to the ventral aspect of the cell and serve as the sites for the cell to degrade underlying matrix proteins (Fig. S2 C). Together, our results indicate that FAK, but not PYK2, is crucial for podosome rosette formation in fibroblasts, endothelial cells, and carcinoma cells.

FAK and PYK2 may regulate different patterning of podosomal organization in

osteoclasts

Mouse RAW264.7 cells can differentiate into osteoclast-like cells by receptor activator of NFκB ligand (RANKL) (Boyle et al., 2003). After induction by RANKL, RAW264.7 cells became multinucleated and their podosomes were mainly organized into a large belt-like structure at the cell periphery (Fig. 1, H and I). However, FAK depletion in RAW264.7 cells impaired this process, keeping podosomes as clusters in the cells (Fig. 1 I). PYK2 depletion also had an adverse effect on the formation of podosome belts in differentiated RAW264.7 cells, which led to podosome rings being the major type of podosome structures in the cells (Fig. 1, H and I). These results suggest that in osteoclasts, FAK may be essential for the cluster-to-ring transition of podosomes, whereas PYK2 may be crucial for the ring-to-belt transition of podosomes.

FAK is dispensable for dot-shaped podosomes, but essential for assembly into rosette-shaped structures

To examine the necessity of FAK in the assembly of podosome rosettes, FAK-null ($FAK^{-/-}$) MEFs and their wild-type (wt) counterparts ($FAK^{+/+}$) were employed in this study (Fig. 2 A). Prior to transformation by v-Src, both $FAK^{+/+}$ and $FAK^{-/-}$ MEFs had almost no podosomes (Fig. 2 B). Strikingly, v-Src induced podosome rosettes only in $FAK^{+/+}$ MEFs, but not in $FAK^{-/-}$ MEFs (Fig. 2 B). However, v-Src induced small dot-shaped podosomes in both

$FAK^{+/+}$ and $FAK^{-/-}$ MEFs to a similar extent (Fig. 2, B-D). These results suggest that while FAK is dispensable for dot-shaped podosomes, it is essential for the assembly of podosome rosettes. Moreover, the formation of podosome rosettes in v-Src-transformed $FAK^{+/+}$ MEFs was correlated with increases in ECM degradation (Fig. 2 E) and Matrigel invasion (Fig. 2 F). The increased invasiveness of v-Src-transformed $FAK^{+/+}$ MEFs was not because of an increase in matrix metalloproteinases (MMPs) (Fig. 2 G).

Elevated expression of FAK is correlated with increases in podosome rosette formation, matrix degradation, and invasion

To further examine the necessity of FAK for the assembly of podosome rosettes, an inducible (Tet-off) FAK expression system was established in v-Src-transformed $FAK^{-/-}$ MEFs (Fig. 3 A). As described in Figure 2, dot-shaped podosomes were already present in v-Src-transformed $FAK^{-/-}$ MEFs before FAK induction. Only upon FAK expression were podosome rosettes allowed to assemble. The extent of podosome rosette formation was correlated with the expression level of FAK (Fig. 3 B). Moreover, the increase in podosome rosettes was correlated with increases in ECM degradation (Fig. 3 C) and invasion (Fig. 3 D). These results together suggest that increased expression of FAK may contribute to v-Src-induced cell invasion, at least in part, through its effect on the induction of podosome rosette assembly.

FAK is localized to podosome rosettes and some dot-shaped podosomes

Confocal microscopic analysis revealed that FAK is co-localized with active Src at podosome rosettes in v-Src-transformed MEFs (Fig. 4, A and B). Like endogenous FAK, green fluorescent protein-fused FAK (GFP-FAK) was found to localize to podosome rosettes. Notably, the COOH domain (aa 687-1053), but not the NH2 domain (aa 1-391), of FAK was localized to podosome rosettes (Fig. 4 C), indicating that the COOH domain of FAK is responsible for its targeting to podosome rosettes.

As described in other types of cells, each podosome has an F-actin core surrounded by focal adhesion proteins such as vinculin (Fig. 4 D). Notably, FAK was found to associate with some, but not all, dot-shaped podosomes (Fig. 4, E and F). The dot-shaped podosomes with FAK association were more potent than those without FAK association in the degradation of ECM proteins (Fig. 4, E and F). These results together indicate that although FAK is dispensable for the formation of dot-shaped podosomes, it is important for their matrix-degrading activity.

The Y397 and catalytic activity of FAK are essential for the triggering of podosome rosette assembly

To examine whether the autophosphorylation site Y397 and catalytic activity of FAK are

required for the induction of podosome rosettes, an inducible (Tet-off) expression for Y397F and Y566F/Y577F mutants was established in v-Src-transformed $FAK^{-/-}$ MEFs. Although the expression levels of both mutants were 3-fold higher than wt FAK (Fig. 5 A), they hardly induced podosome rosettes (Fig. 5 B), indicating that the Y397 and catalytic activity of FAK are required for triggering the assembly of podosome rosettes.

Moreover, the FAK △C mutant with a deletion (aa 687-1053) at its COOH domain was defective in inducing podosome rosettes in v-Src-transformed $FAK^{-/-}$ MEFs (Fig. 5 E). In contrast, the FAK △N mutant with a deletion (aa 1-375) at its NH2 domain was more potent than wt FAK in inducing podosome rosettes (Fig. 5 E). The increased capability of the △N mutant to induce podosome rosettes could be attributed to its increased catalytic activity (Fig. 5 F). We have previously demonstrated that substitution of FAK at Tyr194 with Glu leads to FAK activation (Chen et al., 2011). The Y194E mutant significantly increased the formation of podosome rosettes in CL1-5 cells (Fig. 5, G and H). However, this increase was suppressed by the Src-specific inhibitor PP2 (Fig. 5 H), indicating that the activity of Src is required for FAK to induce the assembly of podosome rosettes.

Interaction of FAK with p130Cas is important for podosome rosette formation

To examine the mechanisms of induction of podosome rosettes by FAK, FLAG epitope-tagged FAK and its various mutants were stably re-expressed in v-Src-transformed

FAK$^{-/-}$ MEFs (Fig. 6 A) and their ability to induce podosome rosettes in those cells was measured (Fig. 6 B). Consistent with the results shown in Figure 5, the Y397F mutant was deficient in inducing podosome rosettes in v-Src-transformed FAK$^{-/-}$ MEFs (Fig. 6 B). The K454R mutant that is defective in ATP binding and thereby has a decreased kinase activity was deficient in inducing podosome rosettes (Fig. 6 B). Notably, the P712A/P715A mutant defective in p130Cas binding (Cary et al., 1998) had an impaired capability to induce podosome rosettes (Fig. 6 B), thus suggesting that interaction of FAK with p130Cas may be crucial for podosome rosette assembly. Accordingly, the tyrosine phosphorylation of p130Cas, but not cortactin and Tks5, was correlated with the expression of FAK in Src-transformed MEFs (Fig. 6 C).

The significance of p130Cas expression in podosome rosettes was demonstrated by knockdown approach (Fig. 6, D and E). However, the constitutively active Y194E mutant of FAK hardly induced p130Cas phosphorylation in SYF (src$^{-/-}$ yes$^{-/-}$ fyn$^{-/-}$) cells (Fig. 6 F), suggesting that FAK may not be the kinase directly phosphorylating p130Cas. Instead, FAK may function as a docking protein for Src to phosphorylate p130Cas. Consistent with this notion, the p130Cas SH3 domain that interferes with the interaction between FAK and p130Cas (Cary et al., 1998) partially suppressed podosome rosettes in Src-transformed 3T3 cells (Fig. 6 G).

Suppression of Rho signaling by FAK is crucial for podosome rosette assembly

FAK has been reported to suppress Rho activity (Ren et al., 2000; Chen et al, 2002). Indeed, the activity of Rho, but not Rac and Cdc42, was inversely correlated with the expression of FAK (Fig. 7 A). Membrane-permeable active Rho (TAT-RhoV14) decreased the formation of podosome rosettes in v-Src-transformed MEFs (Fig. 7 B). In contrast, membrane-permeable C3 exoenzyme (TAT-C3), which specifically ADP-ribosylates and inactivates Rho, rescued the defect in the podosome rosette formation caused by FAK depletion (Fig. 7 B). Thus, FAK may promote podosome rosette formation, at least in part, through its suppression of Rho activity. Indeed, p190RhoGAP was co-localized with FAK at podosome rosettes (Fig. 7 C) and was important for the formation of podosome rosettes (Fig. 7 D). Intriguingly, knockdown of p130Cas increased the Rho activity (Fig. 7 E), suggesting a potential role of p130Cas in Rho inhibition.

Moreover, inhibition of ROCK by the inhibitor Y27632 apparently enhanced the formation of dot-shaped podosomes, but not podosome rosettes, in v-Src-transformed $FAK^{-/-}$ MEFs (Fig. 8, A and B). In contrast, Y27632 significantly promoted the formation of podosome rosettes in v-Src-transformed $FAK^{+/+}$ MEFs (Fig. 8 A), correlated with increases in matrix degradation (Fig. 8 C) and Matrigel invasion (Fig. 8 D). These results not only support that hyper-activation of Rho and ROCK antagonizes the formation of podosome rosettes, but also provide an example to show that increased numbers of dot-shaped

podosomes do not spontaneously trigger the assembly of podosome rosettes in the absence of FAK.

Podosome rosettes are dynamic structures with a lifespan of minutes to hours. The formation of podosome rosettes can be divided into three phases—assembly, maintenance, and disassembly (Fig. 8 E). FAK was found to associate with podosomes in the early assembly phase and then throughout the process (Fig. 8 E). Interestingly, the disassembly of podosome rosettes is always manifested by collapse of the F-actin ring structure towards its center before it is completely dissolved (Fig. 8 E). Y27632 significantly delayed the disassembly phase (Fig. 8 F), suggesting that ROCK may facilitate the disassembly of podosome rosettes.

Microtubule is not necessary for the formation of podosome rosettes in Src-transformed fibroblasts

Microtubule acetylation has been suggested to be important for the formation of podosome belts in osteoclasts (Destaing et al., 2005; Gil-Henn et al., 2007). In particular, in PYK2-null osteoclasts, Rho activity was increased while microtubule acetylation and stability were reduced (Gil-Henn et al., 2007). This raises the possibility that FAK might promote podosome rosettes via regulation of microtubule acetylation. However, we found that although microtubule acetylation was apparently reduced in FAK-null MEFs (Fig. S3 A), it

was not affected by FAK expression and not correlated with the formation of podosome rosettes in Src-transformed MEFs (Fig. S3, B and C). Additionally, we demonstrated that the integrity of microtubules is not necessary for podosome rosette formation in Src-transformed MEFs (Fig. S3 D). Thus, it is possible that microtubule acetylation may only be involved in the ring-to-belt transition of podosomal organization in osteoclasts. This could also explain why PYK2 is essential for the formation of podosome belts, but not podosome rings, in osteoclasts (Fig. 1 I).

Suppression of vimentin filaments by FAK facilitates the assembly of podosome rosettes

ROCK has been implicated to phosphorylate and regulate the organization of the intermediate filaments (Inada et al., 1999). We found that FAK depletion or TAT-RhoV14 addition apparently promoted the organization of the vimentin filaments in CL1-5 cells (Fig. 9 A), concomitant with decreased formation of podosome rosettes (Fig. 9 C). Notably, in the control CL1-5 cells, the vimentin filaments were enriched at the central region of the cells, but were sparse at the cell periphery and the surrounding areas of podosome rosettes (Fig. 9 A). However, the enhanced structure of the vimentin filaments by FAK depletion or TAT-RhoV14 addition extended to the cell periphery (Fig. 9 A) and inhibited the formation of podosome rosettes (Fig. 9 C). Y27632 was able to reverse the effects of FAK

depletion and RhoV14 on vimentin filaments and podosome rosettes (Fig. 9, A and C). More importantly, partial depletion of vimentin was able to compromise the defect in podosome rosette formation caused by FAK depletion or TAT-RhoV14 addition (Fig. 9, B and C). Besides, in CL1-5 cells, the effects of FAK depletion and RhoV14 on vimentin filaments and podosome rosettes were confirmed in Src-transformed MEFs (Fig. S4). These results together suggest that FAK may facilitate the assembly of podosome rosettes through its suppression of Rho/ROCK signaling and vimentin filaments.

S39 and S72 of vimentin have been reported to be the phosphorylation sites for ROCK (Goto et al., 1998). We found that the filament structure of vimentin S39D or S72D mutant was more apparent than that of vimentin S39A or S72A mutant (Fig. 10 B), suggesting that ROCK-mediated phosphorylation of vimentin may facilitate its polymerization. Moreover, partial depletion of vimentin significantly increased the assembly of podosome rosettes in Src-transformed MEFs, which was reversed by re-expression of mCherry fluorescent protein-fused vimentin (cherry-VIM) (Fig. 10 C). Notably, the S39A and S72A mutants were less potent than the S39D and S72D mutants in suppressing podosome rosettes (Fig. 10 C), indicating that less polymerization of vimentin is inversely correlated with more podosome rosette formation. Moreover, the NH2-termianl fragment (aa 1-138) of vimentin that functions as a dominant-negative mutant (Chang et al., 2009) disrupted vimentin filaments (Fig. 10 D) and facilitated the formation of podosome rosettes

(Fig. 10 E). Together, our results suggest that enhanced phosphorylation and polymerization of vimentin by ROCK may antagonize the assembly of podosome rosettes.

Discussion

Podosomes can self-organize into large rosette-like structures in some types of cells. However, the mechanism of how this self-assembly is triggered remains largely unknown. In this study, we identified FAK as a key molecule necessary for the induction of podosome rosette assembly. Our results to support this conclusion are: First, depletion of FAK suppressed the formation of podosome rosettes in Src-transformed fibroblasts, endothelial cells, carcinoma cells, and osteoclasts (Fig. 1 and Fig. S2). Second, oncogenic Src induced the formation of podosome rosettes only in $FAK^{+/+}$ MEFs, but not in $FAK^{-/-}$ MEFs (Fig. 2). Third, dot-shaped podosomes were allowed to assemble into podosome rosettes only upon induction of FAK expression in Src-transformed $FAK^{-/-}$ MEFs (Figs. 3 and 5). Finally, in the absence of FAK, increased numbers of dot-shaped podosomes by the ROCK inhibitor Y27632 did not spontaneously trigger the assembly of podosome rosettes (Fig. 8). All these results support a critical role for FAK in the assembly of podosome rosettes.

The formation of podosome belts is necessary for osteoclasts to perform bone resorption (Boyle et al., 2003). PYK2, the other member of the FAK family, has been reported to be essential for podosome belt formation as well as for bone resorption in osteoclasts (Gil-Henn et al., 2007). In this study, we demonstrated that depletion of FAK

prevents the cluster-to-ring transition of podosomal organization in osteoclasts, while depletion of PYK2 prevents the ring-to-belt transition of podosomal organization in the cells (Fig. 1, H and I). These results suggest that FAK and PYK may coordinately regulate different stages of podosomal organization in osteoclasts. As the cluster-to-ring transition of podosomal organization in osteoclasts is somewhat analogous to podosome rosette assembly in other types of cells, the results derived from osteoclasts also support a critical role for FAK in podosome rosette assembly. However, what is the role of PYK2 in podosome rosette assembly in cells other than osteoclasts? It is apparent that PYK2 is not able to compensate the function of FAK for podosome rosette assembly in MEFs and CL1-5 cells, both of which express high levels of endogenous FAK and PYK2 (Fig. 1). In addition, although PYK2 is hardly detected in NIH3T3 fibroblasts and HUVECs, podosome rosettes can be formed in both types of cells (Fig. 1 and Fig. S2). Thus, our data suggest that FAK, but not PYK2, is crucial for podosome rosette assembly in fibroblasts, endothelial cells, and carcinoma cells.

Podosomes/invadopodia are commonly formed in cancer cells, whereas podosome rosettes appear to be assembled only in some highly invasive cancer cells such as breast cancer BT549 cells (Seals et al., 2005), melanoma RPMI-7951 cells (Seals et al., 2005), pancreatic carcinoma PaCa3 cells (Kocher et al., 2009), and lung adenocarcinoma cells

such as CL1-5 cells (this study) and A549 cells (data not shown). Our results clearly indicate that podosome rosettes are much more potent than dot-shaped podosomes to degrade ECM proteins (Figs. 2, 5, and 8). In addition, elevated expression of FAK is correlated with increases in podosome rosette formation, ECM degradation, and Matrigel invasion (Figs. 3 and 5). Conversely, FAK depletion is concomitant with decreases in podosome rosette formation, ECM degradation, and Matrigel invasion (Figs. 1 and 2; Fig. S2). Therefore, our data strongly suggest a link between FAK, podosome rosettes, and tumor invasion, which may explain, at least in part, why FAK plays an important role in tumor progression to a more malignant phenotype (McLean et al., 2005).

We demonstrated in this study that v-Src induces dot-shaped podosomes both in $FAK^{-/-}$ MEFs and $FAK^{+/+}$ MEFs to a similar extent (Fig. 2), thus supporting that FAK is dispensable for dot-shaped podosomes, in agreement with recent reports describing that FAK is not necessary for the formation of invadopodia in breast cancer cells and colon cancer cells (Vitale et al., 2008; Chan et al., 2009). In contrast, Alexander et al. (2008) reported that FAK is present in invadopodia and essential for invadopodia activity. In this study, we observed that FAK is associated with some, but not all, dot-shaped podosomes in Src-transformed MEFs (Fig. 4). Our findings could reconcile the discrepancy among previous studies that argue whether or not FAK is present in invadopodia. More importantly,

we demonstrate that the dot-shaped podosomes with FAK association are more potent than those without FAK association for ECM degradation (Fig. 4, E and F). However, it is not clear whether dot-shaped podosomes with or without FAK association represents two different stages during the maturation of podosomes or two different subgroups of podosomes with different fates.

As the catalytic activity of FAK is important for its function in promoting podosome rosettes, it is possible that phosphorylation of certain FAK-interacting proteins by FAK may be important for podosome rosette assembly. In accordance with this idea, we found that the tyrosine phosphorylation of p130Cas is selectively regulated by FAK in Src-transformed MEFs, correlated with the formation of podosome rosettes in the cells (Fig. 6 C). In addition, the FAK mutant defective in p130Cas binding is less potent than wt FAK to restore podosome rosettes in Src-transformed $FAK^{-/-}$ MEFs (Fig. 6 B). These results together indicate that the interaction between FAK and p130Cas is important for the induction and/or maintenance of podosome rosettes. In fact, p130Cas and its tyrosine phosphorylation have been reported to be essential for the formation of podosome rosettes (Brábek et al., 2005) and invadopodia (Alexander et al., 2008).

In this study, we demonstrated that FAK promotes the formation of podosome rosettes

in part through its suppression of Rho and ROCK in Src-transformed fibroblasts (Figs. 7, and 8). Activation of the Rho-ROCK signaling pathway has been reported to promote actomyosin-based cell contraction and subsequent podosome dissolution (van Helden et al., 2008). Therefore, it is likely that activation of the Rho-ROCK signaling pathway may facilitate disassembly of podosome rosettes. In this study, we observed that the rosettes-like structure of podosomes always becomes aggregated before it is completely dissolved (Fig. 8 E). This aggregation of F-actin might be because of the increased Rho/ROCK activity and actomyosin-based contraction at podosome rosettes. Consistent with this notion, we found that the ROCK inhibitor Y27632 significantly delayed the disassembly phase of podosome rosettes (Fig. 8 F). In osteoclasts, it has been shown that the formation of podosome belts is disrupted when the Rho activity is high (Destaing et al., 2005).

The dynamics of intermediate filaments can be regulated by Rho signaling (Inada et al., 1999). In this study, we surprisingly found that the organization of vimentin filaments is regulated by FAK in lung carcinoma CL1-5 cells (Fig. 9) and Src-transformed MEFs (Fig. S4). Depletion of FAK apparently enhances the organization of vimentin filaments in the cells, similar to the effect induced by active Rho. As FAK depletion and Rho activation have an adverse effect on the formation of podosome rosettes, our data thus suggest that

enhanced organization of vimentin filaments may be disadvantageous to podosome rosettes. Indeed, fewer or no vimentin filaments are present in the surrounding areas of podosome rosettes (Fig. 9 A). Partial depletion of vimentin rescues the defect in the formation of podosome rosettes caused by FAK depletion or Rho activation (Fig. 9, B and C). Moreover, we found that the S39A and S72A mutants of vimentin are less organized into filaments and less potent in suppressing podosome rosettes than the S39D and S72D mutants (Fig. 10). Thus, our results suggest that enhanced phosphorylation and polymerization of vimentin by ROCK antagonizes the formation of podosome rosettes. A recent study by Schoumacher et al. (2010) described that vimentin filaments penetrate invadopodia at a later stage of invadopodia maturation in carcinoma cells. However, it remains possible that the entry of vimentin filaments to invadopodia might be a mechanism for their disassembly.

In conclusion, we propose that while FAK is dispensable for the formation of dot-shaped podosomes/invadopodia, it is a key molecule necessary for the assembly of podosome rosettes. Tyrosine phosphorylation of p130Cas and suppression of Rho-ROCK signaling by FAK are important for the assembly. Finally, our results highlight that the infiltration of vimentin intermediate filaments may facilitate disassembly of podosome rosettes.

Materials and Methods

Reagents

Polyclonal anti-FAK (A-17), anti-Cdc42, anti-cortactin (H-191), anti-Tks5 (M300), anti-MT1-MMP (L-15) antibodies, monoclonal anti-β tubulin (D-10) antibody, and duplex small-interfering RNA (siRNA) to vimentin were purchased from Santa Cruz Biotechnology (Santa Cruz, CA). Monoclonal anti-FAK (clone 77), anti-p130Cas, anti-PYK2, anti-paxillin, anti-p190RhoGAP, anti-phosphotyrosine (PY20), anti-Rac1, anti-RhoA antibodies, and Matrigel were purchased from BD Biosciences (San Jose, CA). Monoclonal anti-acetylated tubulin (6-11B-1), anti-FLAG, anti-vinculin (clone hVIN-1), anti-vimentin (clone V9 for immunofluorescent staining in human cells), anti-vimentin (clone VIM13.2 for immunefluorescent staining in mouse cells) antibodies, gelatin, nocodazole, and protein A-Sepharose beads were purchased from Sigma-Aldrich (St Louis, MO). Polyclonal anti-MMP9 antibody, monoclonal anti-MMP2, anti-vimentin (for immunoblotting) antibodies and collagen were purchased from Millipore (Billerica, MA). Polyclonal anti-PYK2 antibody was purchased from Cell Signaling Technology (Beverly, MA). Polyclonal anti-FAK pY577 and anti-Src pY416 antibodies were purchased from BioSource (Camarillo, CA). The mouse ascites containing the monoclonal anti-Src (peptide 2–17) produced by hybridoma (CRL-2651) were prepared in our laboratory. Ni-nitrilotriacetic acid (Ni-NTA) agarose

beads and Glutathione Sepharose 4B beads were purchased from GE Healthcare. Fibronectin, phorbol-12-myristate-13-acetate (PMA), puromycin, hygromycin-B, and Y27632 were purchased from Calbiochem (La Jolla, CA). Lipofectamine and Oligofectamine were purchased from Invitrogen (Carlsbad, CA). Fetal bovine serum (FBS) was purchased from Thermo Scientific HyClone (Logan, UT).

Plasmids

The plasmid pGEX-RANKL was kindly provided by Dr. Beth Lee (Ohio State University, Columbus, OH). The plasmid pKH3-FAK encoding HA-FAK was kindly provided by Dr. J. L. Guan (University of Michigan, Ann Arbor, MI). The plasmids pEGFP-FAK and pEGFP-FAK-COOH domain were kindly provided by Dr. D. Ilic (University of California at San Francisco, CA). The plasmids pTAT-His-TAT-RhoV14 and pTAT-His-TAT-C3 were kindly provided by Dr. Z. F. Chang (National Yang-Ming University, Taiwan). The plasmids pBabe-Hygro-p130Cas was kindly provided by Dr. G. S. Goldberg (State University of New York at Stony Brook, NY). The plasmid pEGFP-N1-vimentin was kindly provided by Dr. D. Lev (University of Texas MD Anderson Cancer Center, Houston, TX). The following plasmids were constructed in our laboratory: pEGFP-FAK-NH2 domain (aa. 1-391), pmCherry-FAK, pKH3-FAK nt. C1281A/A1284G (shRNA-resistant mutant), pLKO-AS2.puro-FLAG-FAK series including wt, Y397F, K454R, P712A/715A,

P878A.881A, Y925F, ΔN (deletion of aa. 1-374), and ΔC (deletion of aa. 687-1053), pEGFP-C2-p130Cas SH3 (aa 1-113), and pmCherry-vimentin series including wt, S39A, S39D, S72A, S72D, and N-terminal fragment (aa. 1-138). All mutagenesis was carried out using a QuikChange site-direct mutagenesis kit (Stratagene, La Jolla, CA) and the desired mutations were confirmed by dideoxy DNA sequencing.

Cell culture and transfections

RAW264.7 cells purchased from the American Type Culture Collection were maintained in Dulbecco's modified Eagle's medium (DMEM) supplemented with 10% FBS. To induce differentiation of RAW264.7 cells into osteoclasts, RAW264.7 cells were seeded on glass coverslips coated with collagen for 24 h and then treated with GST-RANKL at 100 ng/ml for 7 days. The multinucleated cells with an enlarged cell morphology were considered as osteoclasts. HUVECs were prepared as described previously (Jaffe et al., 1973) and maintained in M199 supplemented with low serum growth supplements (Invitrogen). $FAK^{+/+}$ MEFs and $FAK^{-/-}$ MEFs were obtained from Dr. D. Ilic (University of California at San Francisco, CA) and maintained as described previously (Chen et al., 2002). Inducible Tet-FAK cells for FAK wt, Y397F, and Y576F/Y577F were obtained from Dr. S. Hanks (Vanderbilt University, Nashville, TN) and maintained as described previously (Chang et al., 2005). To transform cells with v-Src, cells were transfected with pM-vSrc by Lipofectamine

and selected by hygromycin. Lung adenocarcinoma CL1-5 cells were maintained as described previously (Chen and Chen, 2006). To knockdown vimentin in CL1-5 cells, CL1-5 cells were transfected with 66.7 nM duplex siRNA specific to vimentin by Oligofectamine. Three days later, the cells were harvested for analysis.

Lentiviral production and infection

The lentiviral expression system for shRNA was provided by the National RNAi Core Facility, Academia Sinica, Taiwan. For small-hairpin RNA (shRNA)-mediated knockdown, the plasmids pLKO-AS1.puro encoding shRNAs were obtained from the National RNAi Core Facility. The target sequences for FAK are 5'-CCGGTCGAATGATAAGGTGTA-3' (human #1) 5'-GCCCAGGTTTACTGAACTTAA-3' (human #2), 5'-GCCTTAACAATGCGTCAGTTT-3' (mouse #1) and 5'-CGAGTATTAAAGGTCTTTCAT-3' (mouse #2). The target sequences for PYK2 are 5'-CAAGGCTCTCTCATCATCCAT-3' (human) and 5'-GCCTGTCCTTTACACACTCAT-3' (mouse). The target sequence for p130Cas is 5'-CCTCAAGATTCTGGTTGGCAT-3' (mouse). The target sequence for p190A is 5'-CTAAGGCTAGAGGCACTATTA-3' (mouse). The target sequence for vimentin is 5'- GCTTCAAGACTCGGTGGACTT-3' (mouse). For FAK expression, chicken FAK cDNA was amplified by polymerase chain reaction and subcloned in frame to the NheI and AscI site of pLKO-AS2.puro-FLAG vector. To produce

lentiviruses, HEK293T cells were co-transfected with 2.25 μg pCMV-ΔR8.91, 0.25 μg pMD.G, and 2.5 μg pLKO-AS1.puro-shRNA (or pLKO-AS2.puro-FLAG-FAK) by Lipofectamine. After 3 days, the medium containing lentivirus particles was collected and stored at -80°C. The cells were infected with recombinant lentiviruses in the presence of 8 μg/ml polybrene (Sigma-Aldrich) for 24 h. The cells were rinsed by DMEM and allowed to grow in the growth medium for another 48 h. Subsequently, the cells were selected in the growth medium containing 0.5-2.5 μg/ml puromycin for one week and the puromycin-resistant cells were collected for analysis.

Matrix degradation assay

Alexa Fluor 488-conjugated fibronectin and Alexa Fluor 488-conjugated gelatin were prepared as the manufacturer's instructions (Invitrogen). Cells were plated on glass coverslips coated with 20 ng/ml Alexa Fluor 488-conjugated fibronectin or gelatin. After various durations, the cells were fixed and stained for F-actin and nuclei. The areas in which Alexa Fluor 488-conjugated matrix proteins were degraded were measured using Image-Pro Plus software version 5.1(Media Cybemetics, Inc.; Bethesda, MD). A total 10 random fields equivalent to 2 mm^2 were measured.

Matrigel invasion assay

Twenty-four-well transwell chambers (Costar) separated by a membrane with 8-μm pores were coated with 100 μl Matrigel (~2.7 mg/ml). The lower chamber was loaded with 750 μl DMEM with 10% serum. The cells were added to the upper chamber in 250 μl serum-free medium. After 24 h, the cells that had migrated through the Matrigel were fixed by methanol, stained by Giemsa stain and counted.

Immunoprecipitation and immunoblotting

Immunoblotting and immunoprecipitation were performed as described previously (Chen and Chen, 2006). Chemiluminescent signals were detected and quantified using Fuji LAS-3000 luminescence image system.

Small GTPase activity assay

GTP-bound RhoA in whole cell lysates was pulled down by immobilized GST-Rhotekin-RBD. GTP-bound Rac and Cdc42 in whole cell lysates were pulled down by immobilized GST-PAK-RBD. The washed complexes were analyzed by immunoblotting with an antibody specific to RhoA, Rac1, or Cdc42.

Purification of His-tagged TAT-RhoV14 and TAT-C3

His-tagged TAT fusion proteins were expressed in BL21 (DE3) E. coli by isopropyl

β-D-thioglactopyranoside induction. The bacteria were lysed in lysis buffer (6 M Urea, 20 mM Tris pH 7.9, 500 mM NaCl, 5 mM imidazole) and His-tagged TAT fusion proteins were immobilized on Ni-NTA beads. The complexes were washed once with the lysis buffer and twice with washing buffer (20 mM Tris pH 7.9, 500 mM NaCl, 20 mM imidazole), and then eluted by elution buffer (20 mM Tris pH 7.9, 500 mM NaCl, 1 M imidazole). The eluted proteins were dialyzed three times with 200 ml of 5% glycerol in phosphate-buffered saline (PBS) at 4°C for 15 min and stored at -80 °C.

Immunofluorescent staining and laser-scanning confocal fluorescent microscopy

For immunofluorescent staining, cells were fixed by 4% paraformaldehyde in PBS for 30 min at room temperature and permeabilized with 0.05% Triton X-100 in PBS for 10 min at room temperature. To stain vimentin in mouse cells, cells were fixed by cold methanol for 10 min at -20°C and permeabilized with 0.05% Triton X-100 in PBS for 10 min at room temperature. The fixed cells were stained with primary antibodies at 4°C overnight followed by Rhodamine-conjugated or Cy5-conjugated secondary antibodies (Invitrogen) for 3 h at room temperature. The primary antibodies used in immunofluorescent staining in this study were monoclonal anti-acetylated tubulin (1:400), polyclonal anti-cortactin (1:200), polyclonal anti-FAK (1:200), polyclonal anti-Src pY416 (1:400), monoclonal anti-FAK (1:100), monoclonal anti-paxillin (1:200), monoclonal anti-vinculin (1:200), monoclonal

anti-vimentin (clone V9; 1:400), and monoclonal anti-vimentin (clone VIM13.2; 1:200). Rhodamine-conjugated phalloidin and Alexa 488-conjugated phalloidin (Invitrogen) were used to stain actin filaments. Coverslips were mounted in anti-Fade DAPI-Fluoromount-G™ (Southern Biotech; Birmingham, AL) and viewed using a Zeiss LSM510 laser scanning confocal microscope image system with a Zeiss 63X Plan-Apochromat (NA 1.2 W Korr) or a Zeiss 100X Plan-Apochromat objective (NA 1.4 oil).

Time-lapse microscopy

v-Src-transformed $FAK^{+/+}$ cells that stably expressed mCherry-FAK and GFP-actin were grown on glass coverslips coated with 10 μg/ml fibronectin. The cells on the microscope stage were maintained at 37 °C in a humid CO2 atmosphere in a microcultivation system with temperature and CO_2 control devices (Carl Zeiss, Inc.). The cells were monitored on an inverted Zeiss microscope (Axio Observer D1) using a Zeiss 63X Plan-Apochromat objective (NA 1.4 oil). Images were captured every 2 min for 3 h using an AxioCam MRm D digital camera (Carl Zeiss, Inc.) and analyzed by AxioVision Rel. software version 4.8 (Carl Zeiss, Inc.). Wavelengths of 515-560 nm and 450-490 nm were used to excite mCherry and GFP. Beam path filters (BP 590-650 nm and BP 515-565 nm) were used to acquire images for the emission from mCherry and GFP.

Statistics

Statistical analyses were performed by Student's *t* test. Differences were considered to be statistically significant at $P < 0.05$.

Online supplemental material

Fig. 1S shows that podosome rosettes protrude from the ventral surface of cells. Fig. 2S shows that FAK is crucial for podosome rosette formation in Src-transformed NIH3T3 cells and CL1-5 lung carcinoma cells. Fig. 3S shows that microtubules are not necessary for the formation of podosome rosettes in Src-transformed fibroblasts. Fig. 4S shows that FAK may promote podosome rosette formation by suppression of Rho signaling and vimentin filaments in Src-transformed MEFs.

Acknowledgements

We are grateful to Drs. D. Ilic, S. Hanks, Z. F. Chang, D. Lev, and G. S. Goldberg for providing us with reagents. This work was supported by grants NSC97-2628-B-005-001-MY3 and NSC99-2628-B-005-010-MY3 from the National Science Council, Taiwan, and NHRI-EX97-9730BI from the National Health Research Institutes, Taiwan. All authors declare no potential conflict of interest.

Abbreviation

FAK, focal adhesion kinase

ECM, extracellular matrix

SH, Src-homology

ROCK, Rho-associated kinase

MEFs, mouse embryo fibroblasts

HUVECs, human umbilical vein endothelial cells

PMA, phorbol-12-myristate-13-acetate

RANKL, receptor activator of NFkB ligand (RANKL)

GFP, green fluorescent protein

References

Alexander, N.R., K.M. Branch, A. Parekh, E.S. Clark, I.C. Iwueke, S.A. Guelcher, and A.M. Weaver. 2008. Extracellular matrix rigidity promotes invadopodia activity. *Curr. Biol*. 18:1295-1299.

Boyle, W.J., W.S. Simonet, and D.L. Lacey. 2003. Osteoclast differentiation and activation. *Nature*. 423:337-342.

Brábek, J., S.S. Constancio, P.F. Siesser, N.Y. Shin, A. Pozzi, and S.K. Hanks. 2005. Crk-associated substrate tyrosine phosphorylation sites are critical for invasion and metastasis of SRC-transformed cells. *Mol. Cancer Res*. 3:307-315.

Calalb, M.B., T.R. Polte, and S.K. Hanks. 1995. Tyrosine phosphorylation of focal adhesion kinase at sites in the catalytic domain regulates kinase activity: a role for Src family kinases. *Mol. Cell. Biol*. 15:954-963.

Cary, L.A., D.C. Han, T.R. Polte, S.K. Hanks, and J.L. Guan. 1998. Identification of p130Cas as a mediator of focal adhesion kinase-promoted cell migration. *J. Cell Biol*. 140:211-221.

Chan, K.T., C.L. Cortesio, and A. Huttenlocher. 2009. FAK alters invadopodia and focal adhesion composition and dynamics to regulate breast cancer invasion. *J. Cell Biol*. 185:357-370.

Chang, L., K. Barlan, Y.H. Chou, B. Grin, M. Lakonishok, A.S. Serpinskaya, D.K. Shumaker, H. Herrmann, V.I. Gelfand, and R. D. Goldman. 2009. The dynamic properties of intermediate filaments during organelle transport. *J. Cell Sci.* 122:2914-2923.

Chang, L.C., C.H. Huang, C.H. Cheng, B.H. Chen, and H.C. Chen. 2005. Differential effect of the focal adhesion kinase Y397F mutant on v-Src-stimulated cell invasion and tumor growth. *J. Biomed. Sci.* 12:571-585.

Chen, B.H., J.T. Tzen, A.R. Bresnick, and H.C. Chen. 2002. Roles of Rho-associated kinase and myosin light chain kinase in morphological and migratory defects of focal adhesion kinase-null cells. *J. Biol. Chem*. 277:33857-33863.

Chen, S.Y., and H.C. Chen. 2006. Direct interaction of focal adhesion kinase (FAK) with Met is required for FAK to promote hepatocyte growth factor-induced cell invasion. *Mol. Cell. Biol*. 26:5155-5167.

Chen, T.H., P.C. Chan, C.L. Chen, and H.C. Chen. 2011. Phosphorylation of focal adhesion kianse on tyrosine 194 by Met leads to its activation through relief of autoinhibition. *Oncogene* 30:153-166.

Chen, W.T., J.M. Chen, S.J. Parsons, and J.T. Parsons. 1985. Local degradation of fibronectin at sites of expression of the transforming gene product pp60src. *Nature*. 316:156-158.

Destaing, O., F. Saltel, J.C. Geminard, P. Jurdic, and F. Bard. 2003. Podosomes display

actin turnover and dynamic self-organization in osteoclasts expressing actin-green fluorescent protein. *Mol. Biol. Cell*. 14:407-416.

Destaing, O., F. Saltel, B. Gilquin, A. Chabadel, S. Khochbin, S. Ory, and P. Jurdic. 2005. A novel Rho-mDia2-HDAC6 pathway controls podosome patterning through microtubule acetylation in osteoclasts. *J. Cell Sci*. 118:2901-2911.

Gil-Henn, H., O. Destaing, N.A. Sims, K. Aoki, N. Alles, L. Neff, A. Sanjay, A. Bruzzaniti, P. De Camilli, R. Baron, and J. Schlessinger. 2007. Defective microtubule-dependent podosome organization in osteoclasts leads to increased bone density in Pyk2(-/-) mice. *J. Cell Biol*. 178:1053-1064.

Gimona, M., R. Buccione, S. A. Courtneidge, and S. Linder. 2008. Assembly and biological role of podosomes and invadopodia. *Curr. Opin. Cell Biol*. 20:235-241.

Goto, H., H. Kosako, K. Tanabe, M. Yanagida, M. Sakurai, M. Amano, K. Kaibuchi, and M. Inagaki. 1998. Phosphorylation of vimentin by Rho-associated kinase at a unique amino-terminal site that is specifically phosphorylated during cytokinesis. *J. Biol. Chem*. 273:11728-11736.

Guan, J.L., and D. Shalloway. 1992. Regulation of focal adhesion-associated protein tyrosine kinase by both cellular adhesion and oncogenic transformation. *Nature*. 358:690-692.

Ilic, D., Y. Furuta, S. Kanazawa, N. Takeda, K. Sobue, N. Nakatsuji, S. Nomura, J.

Fujimoto, M. Okada, and T. Yamamoto. 1995. Reduced cell motility and enhanced focal adhesion contact formation in cells from FAK-deficient mice. *Nature*. 377:539-544.

Inada, H., H. Togashi, Y. Nakamura, K. Kaibuchi, K. Nagata, and M. Inagaki. 1999. Balance between activities of Rho kinase and type 1 protein phosphatase modulates turnover of phosphorylation and dynamics of desmin/vimentin filaments. *J. Biol. Chem*. 274:34932-34939.

Jaffe, E.A., R.L. Nachman, C.G. Becker, and C.R. Minick. 1973. Culture of human endothelial cells derived from umbilical veins. Identification by morphologic and immunologic criteria. *J. Clin. Invest.* 52:2745-2756.

Kocher, H.M., J. Sandle, T.A. Mirza, N.F. Li, and I.R. Hart. 2009. Ezrin interacts with cortactin to form podosomal rosettes in pancreatic cancer cells. *Gut*. 58:271-284.

Linder, S. 2007. The matrix corroded: podosomes and invadopodia in extracellular matrix degradation. *Trends Cell Biol*. 17:107-117.

Linder, S., and M. Aepfelbacher. 2003. Podosomes: adhesion hot-spots of invasive cells. *Trends Cell Biol*. 13:376-385.

Luxenburg, C., D. Geblinger, E. Klein, K. Anderson, D. Hanein, B. Geiger, and L. Addadi. 2007. The architecture of the adhesive apparatus of cultured osteoclasts: from podosome formation to sealing zone assembly. *PLoS One*. 2:e179.

McLean, G.W., N.O. Carragher, E. Avizienyte, J. Evans, V.G. Brunton, and M.C. Frame. 2005. The role of focal-adhesion kinase in cancer - a new therapeutic opportunity. *Nat. Rev. Cancer*. 5:505-515.

Ren, X.D., W.B. Kiosses, D.J. Sieg, C.A. Otey, D.D. Schlaepfer, and M.A. Schwartz. 2000. Focal adhesion kinase suppresses Rho activity to promote focal adhesion turnover. *J. Cell Sci*. 113:3673-3678.

Schaller, M.D., J.D. Hildebrand, J.D. Shannon, J.W. Fox, R.R. Vines, and J.T. Parsons. 1994. Autophosphorylation of the focal adhesion kinase, pp125FAK, directs SH2-dependent binding of pp60src. *Mol. Cell. Biol*. 14:1680-1688.

Schlaepfer, D.D., S.K. Mitra, and D. Ilic. 2004. Control of motile and invasive cell phenotypes by focal adhesion kinase. *Biochim. Biophys. Acta*. 1692:77-102.

Schoumacher, M., R.D. Goldman, D. Louvard, and D.M. Vignjevic. 2010. Actin, microtubules, and vimentin intermediate filaments cooperate for elongation of invadopodia. *J. Cell Biol*. 189:541-556.

Seals, D.F., E.F. Azucena Jr., I. Pass, L. Tesfay, R. Gordon, M. Woodrow, J.H. Resau, and S.A. Courtneidge. 2005. The adaptor protein Tks5/Fish is required for podosome formation and function, and for the protease-driven invasion of cancer cells. *Cancer Cell*. 7:155-165.

Sieg, D.J., C.R. Hauck, D. Ilic, C.K. Klingbeil, E. Schaefer, C.H. Damsky, and D.D.

Schlaepfer. 2000. FAK integrates growth-factor and integrin signals to promote cell migration. *Nat. Cell Biol*. 2:249-256.

Tatin, F., C. Varon, E. Genot, and V. Moreau. 2006. A signalling cascade involving PKC, Src and Cdc42 regulates podosome assembly in cultured endothelial cells in response to phorbol ester. *J. Cell Sci*. 119:769-781.

van Helden, S.F., M.M. Oud, B. Joosten, N. Peterse, C.G. Figdor, and F.N. van Leeuwen. 2008. PGE2-mediated podosome loss in dendritic cells is dependent on actomyosin contraction downstream of the RhoA-Rho-kinase axis. *J. Cell Sci*. 121:1096-1106.

Vitale, S., E. Avizienyte, V.G. Brunton, and M.C. Frame. 2008. Focal adhesion kinase is not required for Src-induced formation of invadopodia in KM12C colon cancer cells and can interfere with their assembly. *Eur. J. Cell Biol*. 87:569-579.

Webb, B.A., R. Eves, and A.S. Mak. 2006. Cortactin regulates podosome formation: roles of the protein interaction domains. *Exp. Cell Res*. 312:760-769.

Figure Legends

Figure 1. FAK is crucial for podosome rosette assembly in various types of cells. (A) shRNAs specific to FAK (shFAK; clone #1 and clone # 2), PYK2 (shPYK2) or luciferase (shLuc) were stably expressed in v-Src-transformed MEFs. HA-FAK resistant to shFAK was re-expressed into the cells expressing shFAK#1 (shFAK#1/HA-FAK). An equal amount of whole cell lysates was analyzed by immunoblotting with the indicated antibodies. **(B)** The cells were stained for F-actin. The percentage of the cells containing podosome rosettes in the total counted cells ($n \geq 300$) was determined. Values (means $\pm$ s.d.) are from three independent experiments. *$P < 0.005$. **(C)** The cells were subjected to a Matrigel invasion assay. Data were quantified and expressed as a percentage relative to the level of the control. Values (means $\pm$ s.d.) are from three independent experiments. *$P < 0.005$. **(D)** HUVECs and those expressing shRNAs were analyzed by immunoblotting. A monoclonal anti-PYK2 (mAb) and a polyclonal anti-PYK2 (pAb) were used to detect PYK2. **(E)** The cells were treated with (+) or without (-) PMA (100 nM) for 3 h and stained for F-actin. Arrows indicate podosome rosettes. The percentage of the cells containing podosome rosettes in the total counted cells ($n \geq 300$) was determined. Values (means $\pm$ s.d.) are from three independent experiments. *$P < 0.005$. **(F)** shRNAs specific to FAK (shFAK; clone #1 and clone # 2), PYK2 (shPYK2) or luciferase (shLuc) were stably expressed in CL1-5 cells.

HA-FAK resistant to shFAK was re-expressed into the cells expressing shFAK #1 (shFAK#1/HA-FAK). Whole cell lysates were analyzed by immunoblotting with the indicated antibodies. **(G)** The cells were stained for F-acin and the percentage of the cells containing podosome rosettes in the total counted cells ($n \geq 300$) was determined. Values (means ± s.d.) are from three independent experiments. *$P < 0.005$. **(H)** Cell lysates from RAW264.7 cells and those expressing shRNAs were analyzed by immunoblotting with the indicated antibodies. **(I)** The cells were treated with GST-RANKL (100 ng/ml) for 7 days and stained for F-actin and nuclei. Cells containing more than 3 nuclei were defined as osteoclasts. The percentage of the osteoclasts containing podosome clusters, rings or belts in the total counted osteoclasts ($n \geq 100$) was determined. Values (means ± s.d.) are from three independent experiments.

Figure 2. FAK is dispensable for the formation of dot-shaped podosomes, but essential for the assembly of podosome rosettes. (A) Whole cell lysates from $FAK^{+/+}$ MEFs, $FAK^{-/-}$ MEFs, and those transformed by v-Src was analyzed by immunoblotting with the indicated antibodies. **(B)** The percentage of the cells with dot-shaped podosomes and podosome rosettes in the total counted cells ($n \geq 300$) was determined. Values (means ± s.d.) are from three independent experiments. *$P < 0.005$. **(C)** The cells were stained for F-actin and cortactin. Representative high-power images are shown. Arrows indicate

podosome rosettes. Arrowheads indicate dot-shaped podosomes. **(D)** v-Src-transformed MEFs were seeded on Alexa Fluor 488-conjugated fibronectin (FN) for 24 h and then stained for F-actin. The Z-stack images were obtained and reconstituted by confocal microscopy. The *XY* and *XZ* sections of the selected area are shown. Left, dot-shaped podosomes. Right, podosome rosettes. **(E)** The cells were seeded on Alexa Fluor 488-conjugated fibronectin (FN) for 24 h and then stained for F-actin and nuclei. The areas in which FN had been degraded were measured and expressed as –fold relative to the level of $FAK^{+/+}$ MEFs. Values (means ± s.d.) are from three independent experiments. **P* < 0.005. Arrowheads indicate the areas in which FN was degraded by dot-shaped podosomes. Arrows indicate the areas in which FN was degraded by podosome rosettes. **(F)** Matrigel invasion assay. Values (means ± s.d.) are from three independent experiments. **P* < 0.005. **(G)** An equal amount of whole cell lysates was analyzed for MMP expression by immunoblotting.

Figure 3. Increased expression of FAK is correlated with increases in podosome rosette formation, matrix degradation, and cell invasion. (A) An inducible (Tet-off) expression system for wt FAK expression was established in v-Src-transformed $FAK^{-/-}$ MEFs (Tet FAK wt/v-Src). Three cell clones (#2, #7, and #12) were selected and maintained in the medium with (+) tetracycline. The cells were allowed to express FAK

upon tetracycline withdrawal (-). 24 h after tetracycline withdrawal, FAK expression was analyzed by immunoblotting. The expression level of FAK was quantified and expressed as –fold relative to the level of clone #2. **(B)** Three FAK-inducible clones and a control clone (t-TA) that encodes tetracycline-controlled transactivator were grown in the medium with (+) or without (-) tetracycline for 24 h and then stained for F-actin. Arrows indicate podosome rosettes. The percentage of the cells containing podosome rosettes in the total counted cells ($n \geq 300$) was determined. Values (means ± s.d.) are from at least three independent experiments. *$P < 0.005$. $^{\#}P < 0.05$. **(C)** The cells were grown in the medium with (+) or without (-) tetracycline for 24 h and plated on Alexa Fluor 488-conjugated fibronectin (FN) for another 24 h. The areas in which FN was degraded were measured and expressed as –fold relative to the area degraded by clone #2 in the presence of tetracycline. Values (means ± s.d.) are from at least three independent experiments. *$P <$ 0.005. $^{\#}P < 0.05$. **(D)** The cells were grown in the medium with (+) or without (-) tetracycline for 24 h and then subjected to a Matrigel invasion assay. Data were quantified and expressed as –fold relative to the level of clone #2 in the presence of tetracycline. Values (means ± s.d.) are from at least three independent experiments. *$P < 0.005$.

Figure 4. FAK is localized to podosome rosettes and some dot-shaped podosomes.

(A, B) v-Src-transformed $FAK^{+/+}$ MEFs were fixed and stained for F-actin, FAK, paxillin,

and active Src (Src pY416). The Z-stack images were obtained and reconstituted by confocal microscopy. The *XY* and *XZ* sections of the selected area containing a podosome rosette are shown. **(C)** GFP, GFP-FAK, GFP-FAK-NH2 domain, or GFP-FAK-COOH domain was transiently expressed in Src-transformed 3T3 cells and then stained for F-actin. Arrows indicate podosome rosettes. Note that the GFP-FAK-NH2 domain is not localized to podosome rosettes. **(D)** v-Src-transformed MEFs were stained for F-actin, vinculin, and FAK. The representative image shows that FAK and vinculin are localized to dot-shaped podosomes. **(E)** v-Src-transformed $FAK^{+/+}$ MEFs were seeded on Alexa Fluor 488-conjugated fibronectin (FN) for 24 h and then stained for F-actin and FAK. Arrowheads indicate dot-shaped podosomes without FAK association. Arrows indicate dot-shaped podosomes with FAK association. Note that dot-shaped podosomes with FAK association have higher matrix-degrading activity than those without FAK association. **(F)** The cells were seeded on labeled FN for 24 h. The average degraded area by a dot-shaped podosome was measured (n = 15). Values (means ± s.d.) are from three independent experiments. **P* < 0.005.

Figure 5. The Tyr-397 and catalytic activity of FAK are essential for the triggering of podosome rosette assembly. (A) An inducible (Tet-off) expression system for FAK and its mutants was established in v-Src-transformed $FAK^{-/-}$ MEFs. The cells were maintained in

the medium with (+) tetracycline. 24 h after tetracycline withdrawal (-), the cells were lysed and analyzed by immunoblotting. **(B)** The cells were grown in the absence of tetracycline for 24 h and stained for F-actin. Arrows indicate podosome rosettes. The percentage of the cells containing podosome rosettes in the total counted cells ($n \geq 300$) was determined. Values (means ± s.d.) are from three independent experiments. *$P < 0.005$. **(C)** The cells were grown in the presence (+) or absence (-) of tetracycline for 24 h and then subjected to a matrix degradation assay in the presence of tetracycline. Data were quantified and expressed as –fold relative to the level of the t-TA clone in the presence of tetracycline. Values (means ± s.d.) are from at least three independent experiments. *$P < 0.005$. **(D)** The cells were grown in the presence (+) or absence (-) of tetracycline for 24 h and then subjected to a Matrigel invasion assay. Data were quantified and expressed as –fold relative to the level of the t-TA clone in the presence of tetracycline. Values (means ± s.d.) are from three independent experiments. *$P < 0.005$. **(E)** FLAG-FAK or its mutants with deletion at the NH2 domain (ΔN) or the COOH domain (ΔC) were stably expressed in v-Src-transformed $FAK^{-/-}$ MEFs. An equal amount of whole cell lysates was analyzed by immunoblotting with the indicated antibodies. The formation of podosome rosettes was quantified and expressed as –fold relative to that of the cells expressing FLAG-FAK wt. Values (means ± s.d.) are from three independent experiments. *$P < 0.005$. **(F)** The Y577 phosphorylation of FLAG-FAK was analyzed by immunoblotting. Data were normalized to

the protein level and expressed as –fold relative to the level of FAK wt. Values are the average from two independent experiments. **(G)** Stable expression of T7-FAK and Y194E mutant in CL1-5 cells. **(H)** The cells were treated with (+) or without (-) PP2 at 10 μM for 1 h and stained for F-actin. The formation of podosome rosettes was quantified and expressed as a percentage relative to the control cells (neo) in the absence of PP2. Values (means ± s.d.) are from three independent experiments. *P < 0.005.

Figure 6. Interaction of FAK with p130Cas is important for podosome rosette formation. (A) Stable expression of FLAG-FAK and its mutants in v-Src-transformed $FAK^{-/-}$ MEFs. **(B)** The formation of podosome rosettes was quantified and expressed as a percentage relative to the cells expressing FLAG-FAK wt. Values (means ± s.d.) are from three independent experiments. *P < 0.005. **(C)** FAK was depleted in v-Src-transformed $FAK^{+/+}$ MEFs by shRNA (shFAK). Subsequently, HA-FAK resistant to shFAK was stably re-expressed into the FAK-depleted cells (shFAK/HA-FAK). The tyrosine phosphorylation of p130Cas (Cas), cortactin, and Tks5 were analyzed. The tyrosine phosphorylation of p130Cas was quantified and expressed as a percentage relative to the level in the cells expressing shLuc. The results shown are representative of three experiments. **(D)** Immunoblotting for the p130Cas expression in v-Src-transformed MEFs and those expressing shRNAs specific to p130Cas (shCas) or luciferase (shLuc) as a control. **(E)** The

cells were stained for F-actin and the percentage of the cells containing podosome rosettes in the total counted cells ($n \geq 300$) was determined. Values (means ± s.d.) are from three independent experiments. *$P < 0.005$. **(F)** T7-FAK Y194E or c-SrcY527F was transiently expressed in SYF cells and the tyrosine phosphorylation of p130Cas (Cas pY) was analyzed. **(G)** GFP or GFP-p130Cas SH3 domain (GFP-Cas SH3) was transiently expressed in Src-transformed 3T3 cells. The cells were stained for F-actin and the percentage of the cells containing podosome rosettes in the total counted cells expressing GFP or GFP-Cas SH3 ($n \geq 100$) was determined. Values (means ± s.d.) are from three independent experiments. *$P < 0.005$.

Figure 7. Suppression of Rho signaling by FAK is crucial for podosome rosette assembly. (A) The levels of active (GTP-bound) Rho family proteins including RhoA, Rac1, and Cdc42 in the cells were measured. The results shown are representative of three experiments. **(B)** v-Src-transformed MEFs expressing shRNA to luciferase (shLuc) were treated with TAT-RhoV14 at various concentrations for 12 h. v-Src-transformed MEFs expressing shRNA to FAK (shFAK) were treated with TAT-C3 at various concentrations for 12 h. The formation of podosome rosettes was measured and expressed as a percentage relative to that of control cells expressing shLuc. Values (means ± s.d.) are from three independent experiments. $^{\#}P < 0.005$ (compared to the shLuc cells without TAT-RhoV14

treatment). *P < 0.005 (compared to the shFAK cells without TAT-C3 treatment). **(C)** Src-transformed 3T3 cells were stained for F-actin, p190RhoGAP (p190A), and FAK. The *Z*-stack images were obtained and reconstituted by confocal microscopy. The *XY* and *XZ* sections of the selected area containing a podosome rosette are shown. **(D)** v-Src-transformed MEFs and those expressing shRNAs specific to FAK (shFAK), p190RhoGAP (shp190A) or luciferase (shLuc) were analyzed for the expression of FAK and p190RhoGAP (p190A) by immunoblotting. The level of active RhoA was measured. The formation of podosome rosettes was measured and expressed as a percentage relative to that of the control cells expressing shLuc. Values (means ± s.d.) are from three independent experiments. *P < 0.005. **(E)** The effect of p130Cas knockdown on Rho activity was analyzed. The level of active RhoA was measured, quantified, and expressed as –fold relative to the control cells. The results shown are the representative of three experiments.

Figure 8. ROCK facilitates the disassembly of podosome rosettes. (A) v-Src-transformed $FAK^{-/-}$ and $FAK^{+/+}$ MEFs were treated with (+) or without (-) the ROCK inhibitor Y27632 (10 μM) for 2 h. The percentage of the cells containing dot-shaped podosomes (blue bars) or podosome rosettes (red bars) in the total counted cells ($n \geq 300$) was determined. Values (means ± s.d.) are from at least three independent experiments.

*P < 0.005. **(B)** v-Src-transformed FAK$^{-/-}$ MEFs were treated with (+) or without (–) 10 μM Y27632 for 2 h and stained for F-actin and cortactin. Representative high-power images are shown. **(C)** The cells were seeded on Alexa Fluor 488-conjugated fibronectin (FN) for 24 h and then treated with (+) or without (-) Y27632 for another 6 h. The areas in which FN had been degraded were measured. Data are expressed as –fold relative to the level of v-Src-transformed FAK$^{-/-}$ MEFs in the absence of Y27632. Values (means ± s.d.) are from three independent experiments. *P < 0.005. $^{\#}P$ < 0.05. **(D)** The cells were subjected to a Matrigel invasion assay in the presence (+) or absence (-) of 10 μM Y27632. Data are expressed as –fold relative to the level of v-Src-transformed FAK$^{-/-}$ MEFs in the absence of Y27632. Values (means ± s.d.) are from three independent experiments. *P < 0.005. **(E)** v-Src-transformed FAK$^{+/+}$ MEFs stably expressing mCherry-FAK and GFP-actin were monitored by time-lapse microscopy. Representative sequential images selected at different time points are shown. **(F)** v-Src-transformed FAK$^{+/+}$ MEFs stably expressing mCherry-FAK and GFP-actin were monitored by time-lapse microscopy in the presence (+) or absence (-) of 10 μM Y27632. The duration (means ± s.d.) of the disassembly phase in the total counted podosome rosettes (n = 15) was determined. *P < 0.005.

Figure 9. Suppression of vimentin filaments by FAK facilitates the assembly of podosome rosettes. (A) shRNAs specific to FAK (shFAK) or luciferase (shLuc) as a

control were stably expressed in CL1-5 cells. The control cells were treated with 1 μg/ml TAT-RhoV14 for 12 h. In some cases, the cells were further treated with 10 μM Y27632. The cells were stained for F-actin, vimentin (VIM), and nuclei. The selected areas from the images were enlarged. For the control cells, enlarged images from a podosome rosette (a) and the cell periphery (b) are shown. The fluorescent intensity of vimentin filaments per cell was measured (n = 30) and expressed as –fold relative to the level of the control cells. *P < 0.005. $^{\#}P$ < 0.05. **(B)** The CL1-5 cells expressing shFAK were transfected with duplex siRNA specific to vimentin (shFAK/siVIM). After 3 days, CL1-5 cells and those transfected with vimentin siRNA were treated with 1 μg/ml TAT-RhoV14 for 12 h. The expression of FAK and vimentin was analyzed by immunoblotting. **(C)** The cells were stained for F-actin. The formation of podosome rosettes was quantified. Values (means ± s.d.) are from three independent experiments. *P < 0.005. $^{\#}P$ < 0.05.

Figure 10. Phosphorylation and polymerization of vimentin by ROCK antagonizes the formation of podosome rosettes. (A) Vimentin was depleted in v-Src-transformed $FAK^{+/+}$ MEFs by shRNA (shVIM). Subsequently, mCherry-vimentin (cherry-VIM) or its mutants were stably re-expressed in the vimentin-depleted cells (shVIM/cherry-VIM). The expression of vimentin was analyzed by immunoblotting. **(B)** The organization of mCherry-vimentin in the cells was visualized under a

fluorescent microscope (Leica DML). The selected areas from the images were enlarged. **(C)** The formation of podosome rosettes was measured and expressed as a percentage relative to the control cells. Values (means ± s.d.) are from three independent experiments. $^{*}P < 0.005$. $^{\#}P < 0.05$. **(D)** mCherry-vimentin or its NH2-terminal fragment (aa. 1-138) was transiently expressed in Src-transformed 3T3 cells. The cells were stained for vimentin (VIM). **(E)** The percentage of the cells containing podosome rosettes in the total counted cells expressing mCherry proteins ($n \geq 100$) was determined. Values (means ± s.d.) are from three independent experiments. $^{*}P < 0.005$. $^{\#}P < 0.05$. **(F)** Diagram illustrating that FAK may facilitate the assembly of podosome rosettes by promotion of p130Cas phosphorylation and suppression of the Rho-ROCK-vimentin pathway.

Supplemental materials

FAK Is Required for Assembly of Podosome Rosettes

Yi-Ru Pan, Chien-Lin Chen, and Hong-Chen Chen

Supplemental figure legends

Figure S1. Podosome rosettes protrudes from the ventral surface of cells

(A) v-Src-transformed MEFs were grown on fibronectin-coated glass coverslips for 24 h and then stained for F-actin. A representative 3D image is shown, which are reconstituted from 37 confocal slices at 1 micron intervals using LSM imaging software. The *XZ* section and *YZ* section at indicated position are shown. Bar, 20 μm. **(B)** The three-dimensional image as shown in panel A was converted into motion 4D images using LSM510 VisArt4D® software (Carl Zeiss). Two representative frames are shown. **(C)** Diagram depicting the structure of podosome rosettes. Values (mean ± s.d.) are from 50 podosome rosettes. Note that approximately one third of the structure is below the ventral surface of cells. **(D)** v-Src-transformed MEFs were grown on fibronectin-coated glass coverslips for 24 h and then stained for F-actin. The images were captured by total internal reflection fluorescence (TIRF) microscopy.

Figure S2. FAK is crucial for podosome rosettes in SrcY527F-transformed NIH3T3 cells

and human lung adenocarcinoma CL1-5 cells

(A) SrcY527F-transformed NIH3T3 cells were infected with recombinant lentiviruses encoding shRNAs specific to FAK (shFAK) or luciferase (shLuc) as a control. **(B)** The cells as in panel (A) were stained for F-actin. Arrows indicate podosome rosettes. The percentage of the cells with podosome rosettes in the total counted cells was determined. Values (means ± s.d.) are from three independent experiments. *P < 0.005. **(C)** CL1-5 cells were grown on glass coverslips coated with Alexa Fluor 488-conjugated gelatin for 24 h and then stained for F-actin. Representative images from the XY and XZ sections are shown. **(D, E)** CL1-5 cells were grown on gelatin-coated glass coverslips and stained for F-actin, cortactin, and FAK. Cortactin served as a marker for podosomes. **(F)** Control CL1-5 cells and those expressing shLuc, shFAK, or shPYK2 were subjected to an Matrigel invasion assay. Data were quantified and expressed as a percentage relative to the level of the control CL1-5 cells, which was defined as 100%. Values (means ± s.d.) are from three independent experiments. *P < 0.005.

Figure S3. Assembly of podosome rosettes is independent of the acetylation or integrity of microtubules

(A) An equal amount of whole cell lysates from v-Src-transformed $FAK^{+/+}$ MEFs and v-Src-transformed $FAK^{-/-}$ MEFs was analyzed by immunoblotting with antibodies as indicated. The cells were grown on fibronectin for 24 h and stained for F-actin and acetylated tubulin.

Representative images from three independent experiments are shown. **(B)** An inducible (Tet-off) expression system for the expression of FAK was constructed in v-Src-transformed $FAK^{-/-}$ MEFs (Tet FAKwt/ v-Src). The cells were grown on coverslips in the medium with (+) or without (-) tetracycline for 24 h. The expression of FAK and acetylated tubulin was analyzed by immunoblotting. The cells were fixed and stained for F-actin and acetylated tubulin. **(C)** v-Src-transformed MEFs were infected with recombinant lentiviruses encoding shRNAs specific to FAK (shFAK) or luciferase (shLuc) as a control. The expression of FAK and acetylated tubulin was analyzed by immunoblotting. Those cells were grown on fibronectin for 24 h and stained for F-actin and acetylated tubulin. **(D)** v-Src-transformed MEFs were grown on fibronectin-coated glass coverslips for 24 h and their cytoskeleton including both actin filaments and microtubules were disrupted by cold shock (at 4 °C for 2h) and then recovered at 37 °C for 24 h in the presence of 10 μg/ml nocodazole (NOC) or the control solvent dimethyl sulfoxide (DMSO). The cells were fixed and stained for F-actin and β-tubulin.

Figure S4. FAK may promote podosome rosette formation by suppression of Rho signaling and vimentin filaments

(A) v-Src-transformed MEFs were infected with recombinant lentiviruses encoding shRNAs specific to FAK (shFAK). The cells expressing shFAK were treated with or without 10 μM Y27632 for 12 h. v-Src-transformed MEFs were treated with 5 μg/ml TAT-RhoV14 for 12 h

and then treated with or without 10 μM Y27632 for 12 h. Those cells were fixed and stained for vimentin. The fluorescence intensity of vimentin filaments per cell was measured using the AlxioVision Rel. software (version 4.8) (n=30) and expressed as –fold relative to the level of the control. Values (means ± s.d.) are from three independent experiments. *$P < 0.005$. $^{\#}P < 0.05$. **(B)** The cells as described in panel (A) were grown on fibronectin-coated glass coverslips for 24 h and stained for F-actin. The podosome rosette formation was quantified and expressed as percentage relative to the level of the control. Values (means ± s.d.) are from three independent experiments. *$P < 0.005$.

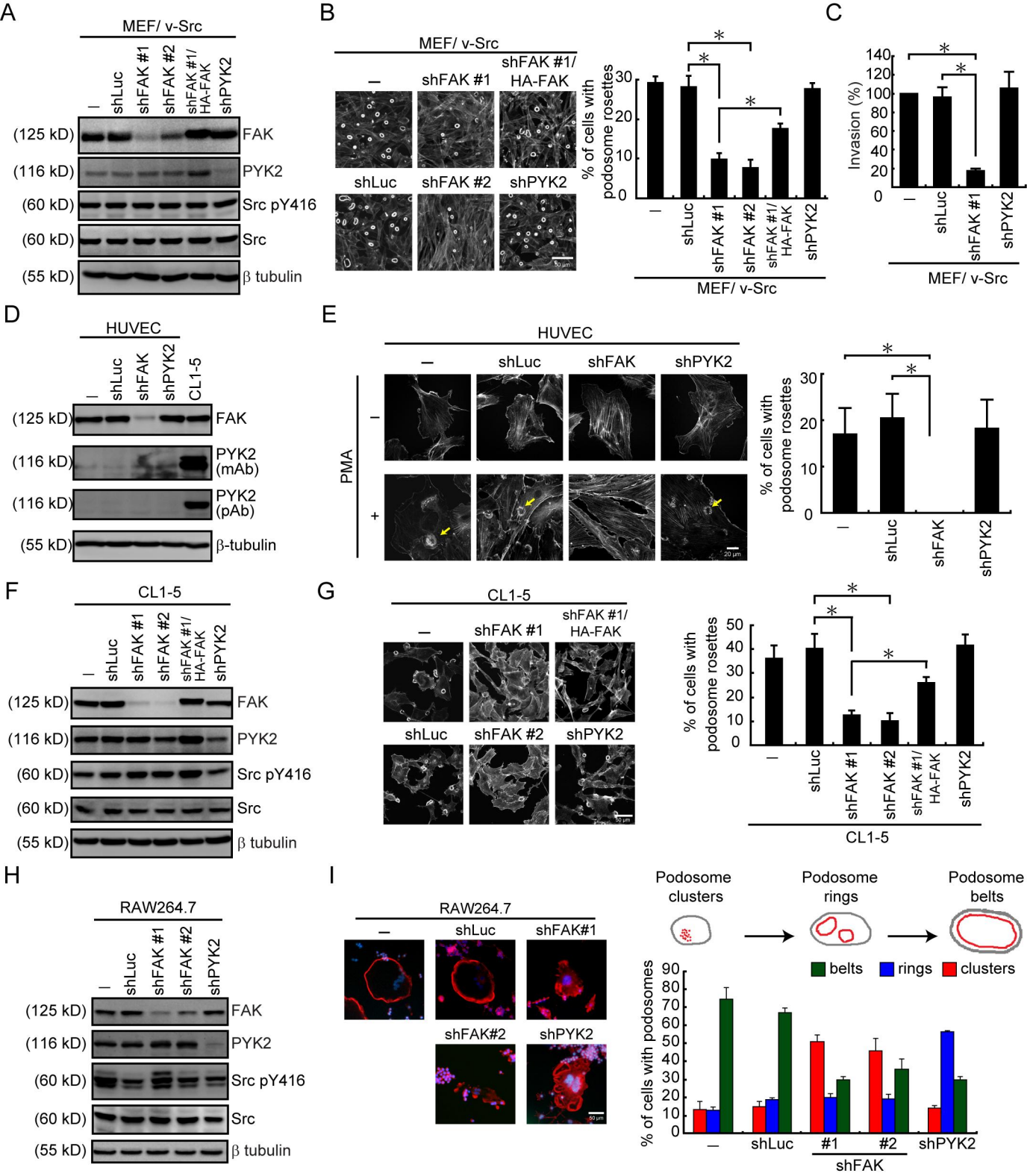
A
MEF/ v-Src
–
shLuc
shFAK #1
shFAK #2
shFAK #1/ HA-FAK
shPYK2
(125 kD)
FAK
(116 kD)
PYK2
(60 kD)
Src pY416
(60 kD)
Src
(55 kD)
β tubulin
B
MEF/ v-Src
shFAK #1/ HA-FAK
shLuc
shFAK #2
shPYK2
% of cells with podosome rosettes
MEF/ v-Src
C
Invasion (%)
MEF/ v-Src
D
HUVEC
CL1-5
(116 kD)
PYK2 (mAb)
PYK2 (pAb)
β-tubulin
E
HUVEC
shFAK
PMA
F
CL1-5
G
CL1-5
H
RAW264.7
I
RAW264.7
Podosome clusters
Podosome rings
Podosome belts
belts
rings
clusters
% of cells with podosomes
shFAK

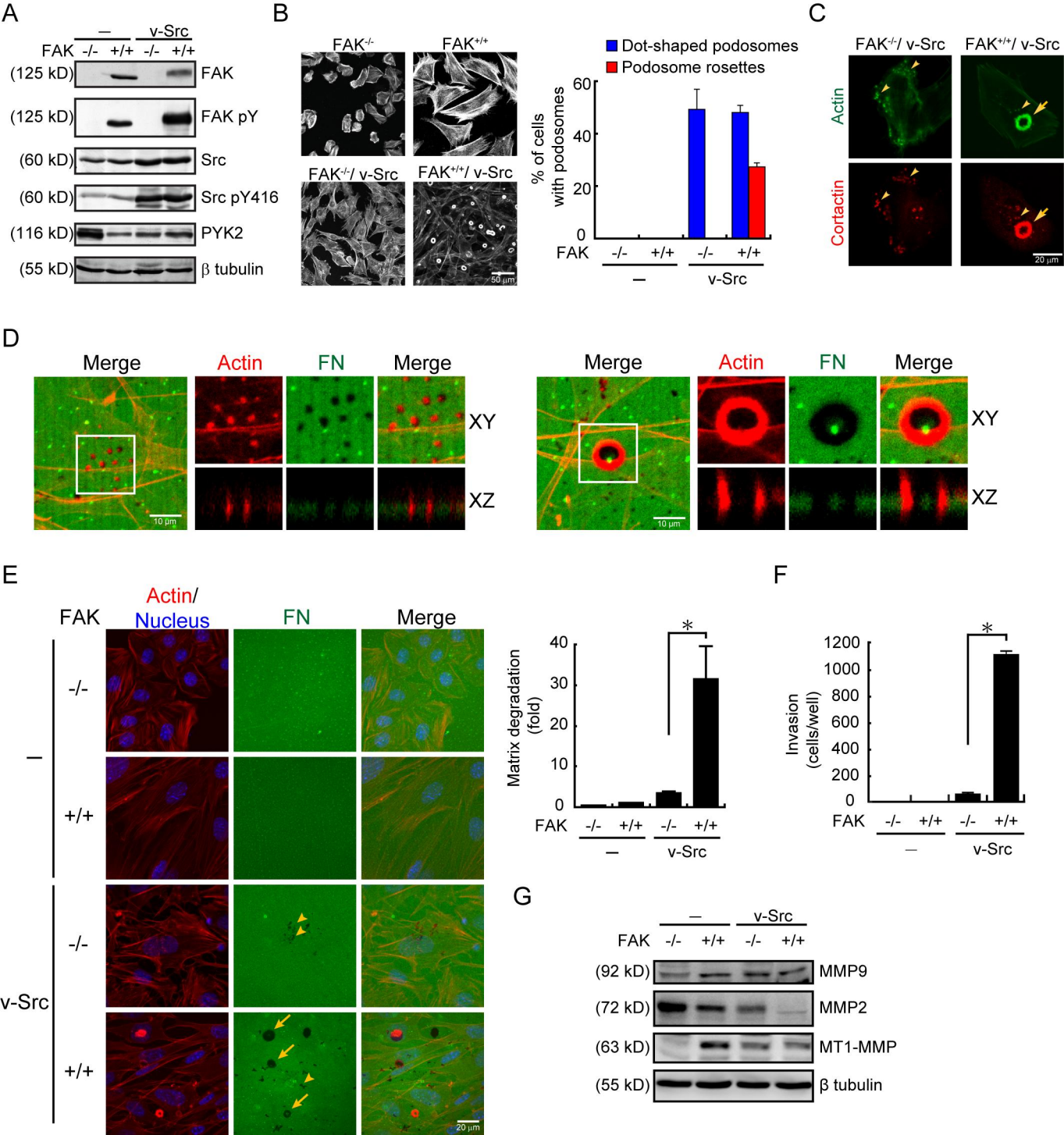
A
—
v-Src
FAK -/- +/+ -/- +/+
(125 kD) FAK
(125 kD) FAK pY
(60 kD) Src
(60 kD) Src pY416
(116 kD) PYK2
(55 kD) β tubulin
B
FAK-/-
FAK+/+
FAK-/- v-Src
FAK+/+ v-Src
50 μm
Dot-shaped podosomes
Podosome rosettes
% of cells with podosomes
60
40
20
0
FAK -/- +/+ -/- +/+
—
v-Src
C
FAK-/- v-Src
FAK+/+ v-Src
Actin
Cortactin
20 μm
D
Merge
Actin
FN
Merge
XY
XZ
10 μm
E
FAK
Actin/ Nucleus
FN
Merge
—
v-Src
-/-
+/+
20 μm
Matrix degradation (fold)
40
30
20
10
0
*
FAK -/- +/+ -/- +/+
—
v-Src
F
Invasion (cells/well)
1200
1000
800
600
400
200
0
*
FAK -/- +/+ -/- +/+
—
v-Src
G
—
v-Src
FAK -/- +/+ -/- +/+
(92 kD) MMP9
(72 kD) MMP2
(63 kD) MT1-MMP
(55 kD) β tubulin

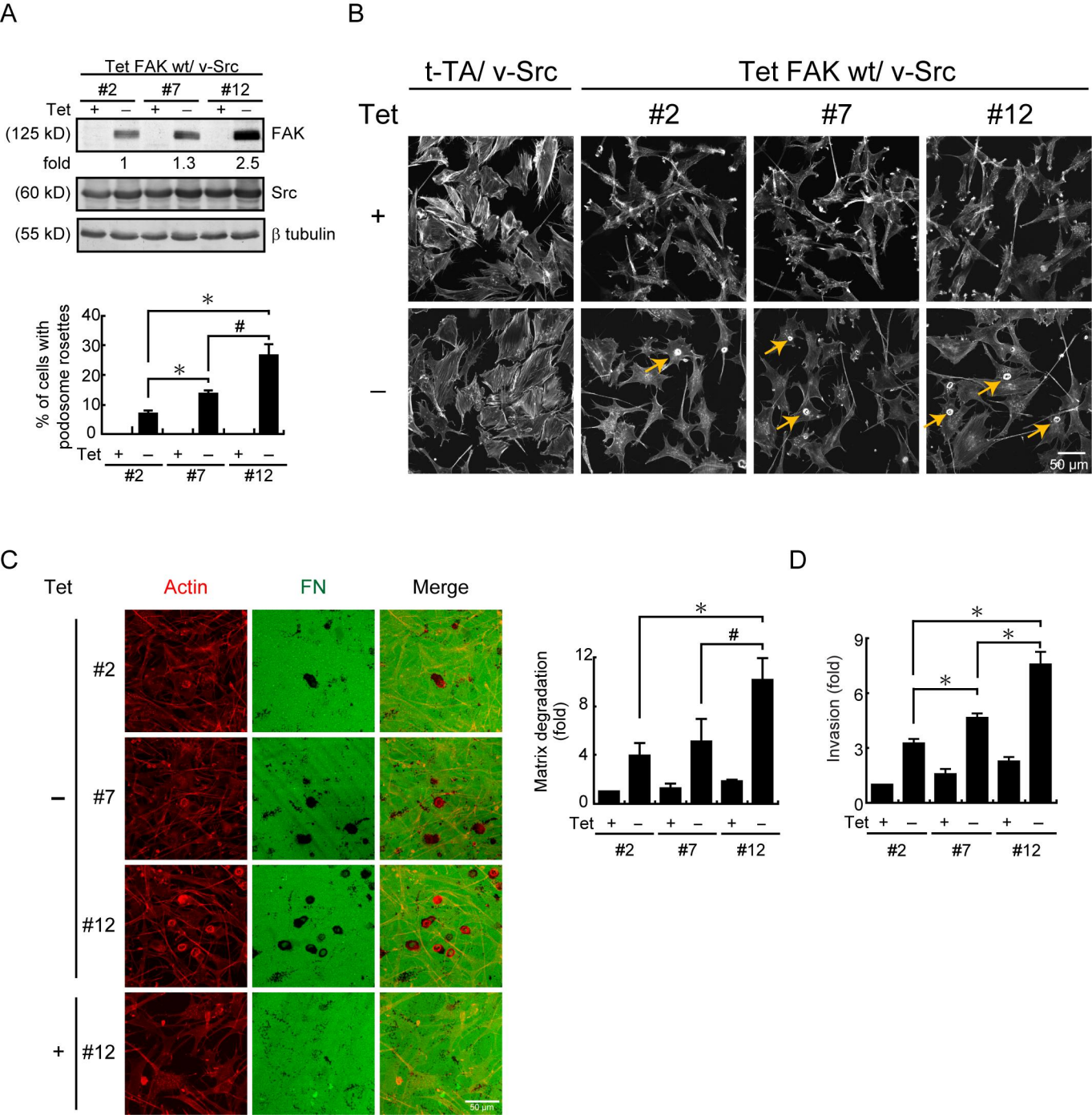
A
Tet FAK wt/ v-Src
#2
#7
#12
Tet
+
–
(125 kD)
FAK
fold
1
1.3
2.5
(60 kD)
Src
(55 kD)
β tubulin
% of cells with podosome rosettes
40
30
20
10
0
*
#
B
t-TA/ v-Src
Tet FAK wt/ v-Src
Tet
#2
#7
#12
+
–
50 μm
C
Tet
Actin
FN
Merge
#2
#7
#12
–
+
50 μm
Matrix degradation (fold)
12
8
4
0
D
Invasion (fold)
9
6
3
0

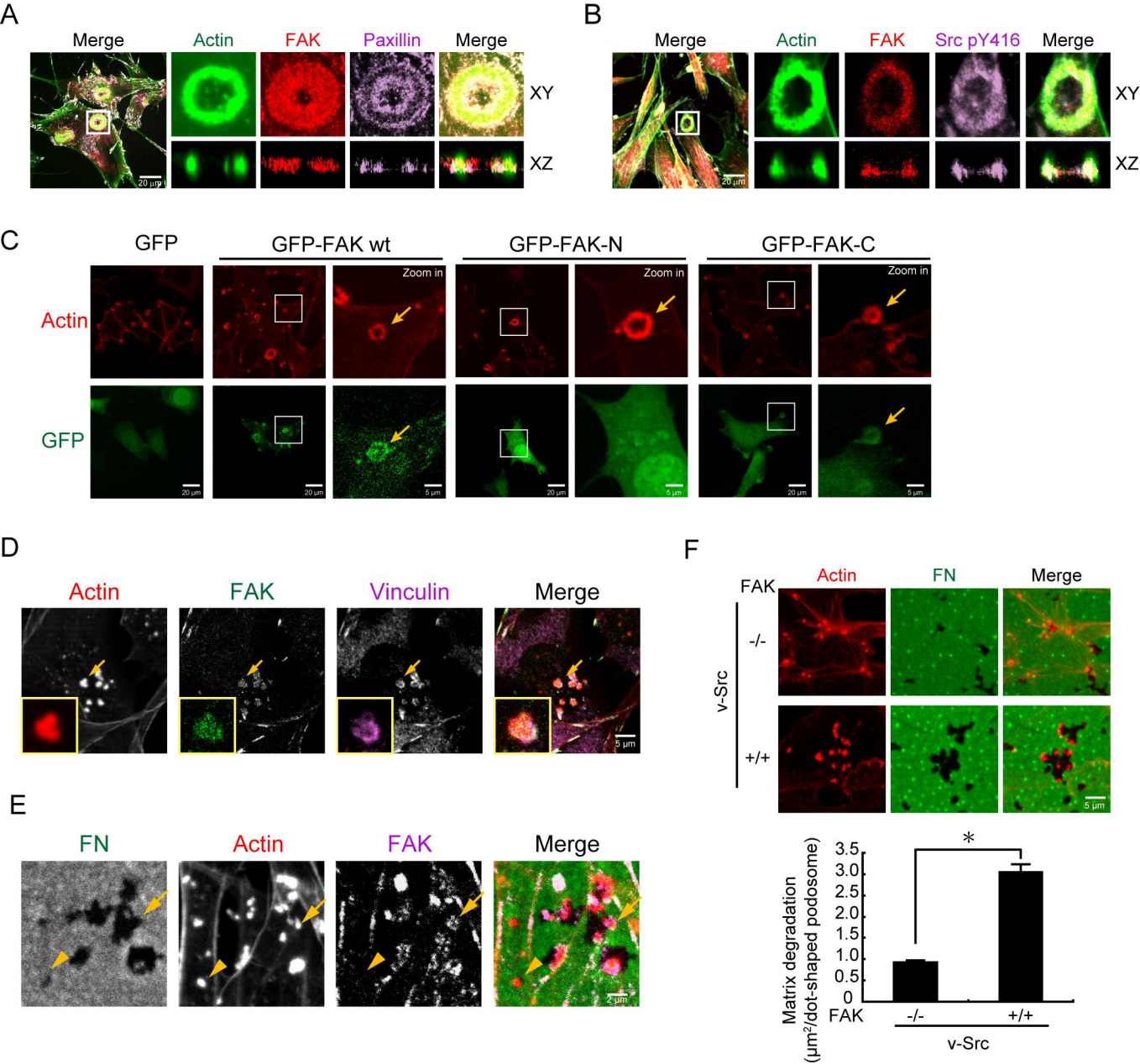
A
Merge
Actin
FAK
Paxillin
Merge
XY
XZ
B
Merge
Actin
FAK
Src pY416
Merge
XY
XZ
C
GFP
GFP-FAK wt
GFP-FAK-N
GFP-FAK-C
Zoom in
Actin
GFP
D
Actin
FAK
Vinculin
Merge
E
FN
Actin
FAK
Merge
F
FAK
Actin
FN
Merge
v-Src
-/-
+/+
Matrix degradation (μm²/dot-shaped podosome)
3.5
3.0
2.5
2.0
1.5
1.0
0.5
0
*
FAK
-/-
+/+
v-Src

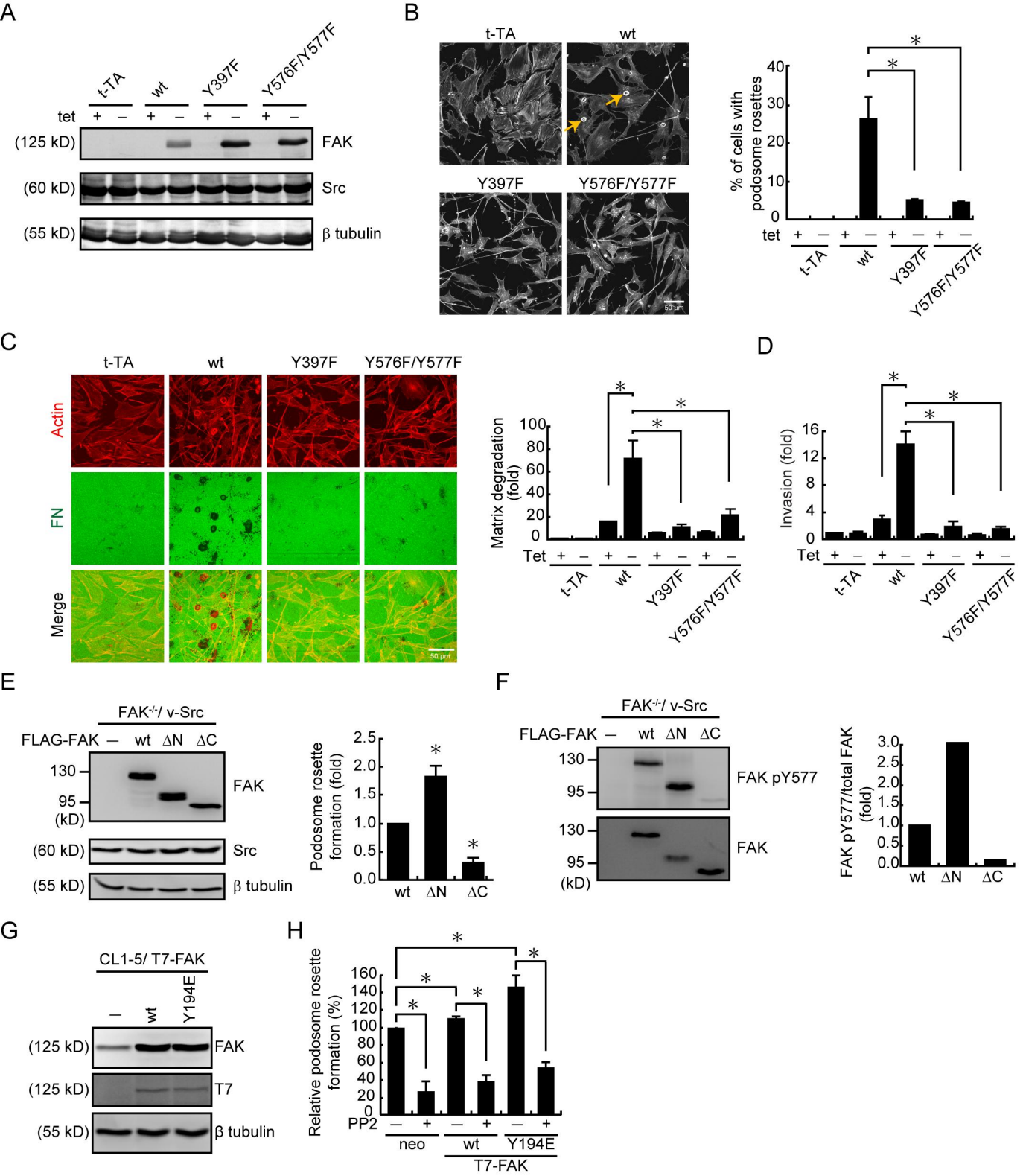
A
t-TA
wt
Y397F
Y576F/Y577F
tet + – + – + – + –
(125 kD)
FAK
(60 kD)
Src
(55 kD)
β tubulin
B
t-TA
wt
Y397F
Y576F/Y577F
50 μm
% of cells with podosome rosettes
40
30
20
10
0
*
*
tet + – + – + – + –
t-TA
wt
Y397F
Y576F/Y577F
C
t-TA
wt
Y397F
Y576F/Y577F
Actin
FN
Merge
50 μm
Matrix degradation (fold)
100
80
60
40
20
0
*
*
*
Tet + – + – + – + –
t-TA
wt
Y397F
Y576F/Y577F
D
Invasion (fold)
16
12
8
4
0
*
*
*
Tet + – + – + – + –
t-TA
wt
Y397F
Y576F/Y577F
E
FAK-/- / v-Src
FLAG-FAK — wt ΔN ΔC
130
95
(kD)
FAK
(60 kD)
Src
(55 kD)
β tubulin
Podosome rosette formation (fold)
2.5
2.0
1.5
1.0
0.5
0.0
*
*
wt
ΔN
ΔC
F
FAK-/- / v-Src
FLAG-FAK — wt ΔN ΔC
130
95
FAK pY577
130
95
(kD)
FAK
FAK pY577/total FAK (fold)
3.0
2.5
2.0
1.5
1.0
0.5
0.0
wt
ΔN
ΔC
G
CL1-5/ T7-FAK
—
wt
Y194E
(125 kD)
FAK
(125 kD)
T7
(55 kD)
β tubulin
H
Relative podosome rosette formation (%)
160
140
120
100
80
60
40
20
0
*
*
*
*
*
PP2 — + — + — +
neo
wt
Y194E
T7-FAK

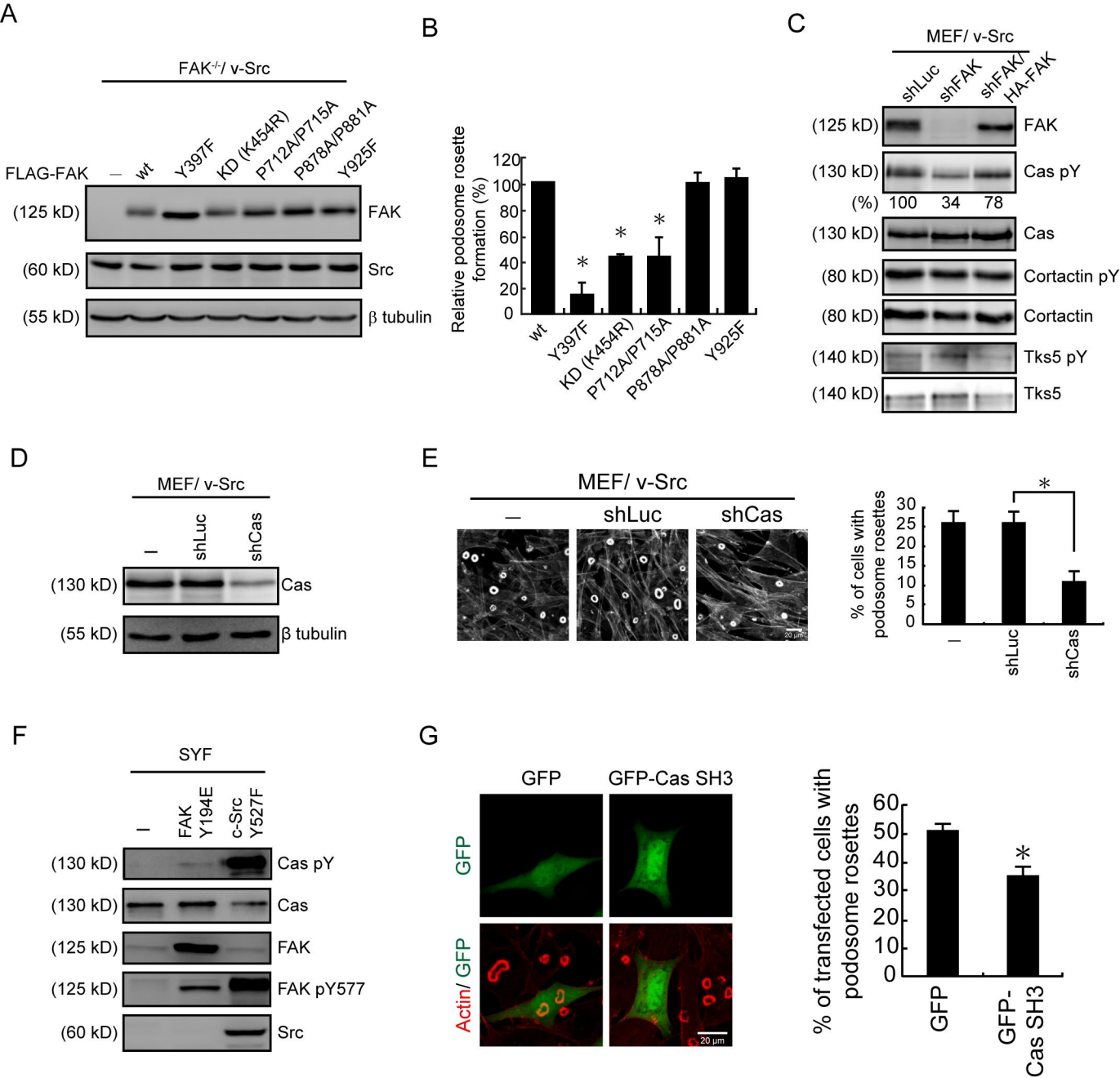
A
FAK-/- / v-Src
FLAG-FAK
—
wt
Y397F
KD (K454R)
P712A/P715A
P878A/P881A
Y925F
(125 kD)
FAK
(60 kD)
Src
(55 kD)
β tubulin
B
Relative podosome rosette formation (%)
120
100
80
60
40
20
0
*
wt
Y397F
KD (K454R)
P712A/P715A
P878A/P881A
Y925F
C
MEF/ v-Src
shLuc
shFAK
shFAK/ HA-FAK
(125 kD)
FAK
(130 kD)
Cas pY
(%) 100 34 78
(130 kD)
Cas
(80 kD)
Cortactin pY
(80 kD)
Cortactin
(140 kD)
Tks5 pY
(140 kD)
Tks5
D
MEF/ v-Src
—
shLuc
shCas
(130 kD)
Cas
(55 kD)
β tubulin
E
MEF/ v-Src
—
shLuc
shCas
20 μm
% of cells with podosome rosettes
30
25
20
15
10
5
0
*
—
shLuc
shCas
F
SYF
—
FAK Y194E
c-Src Y527F
(130 kD)
Cas pY
(130 kD)
Cas
(125 kD)
FAK
(125 kD)
FAK pY577
(60 kD)
Src
G
GFP
GFP-Cas SH3
GFP
Actin/ GFP
20 μm
% of transfected cells with podosome rosettes
60
50
40
30
20
10
0
*
GFP
GFP-Cas SH3

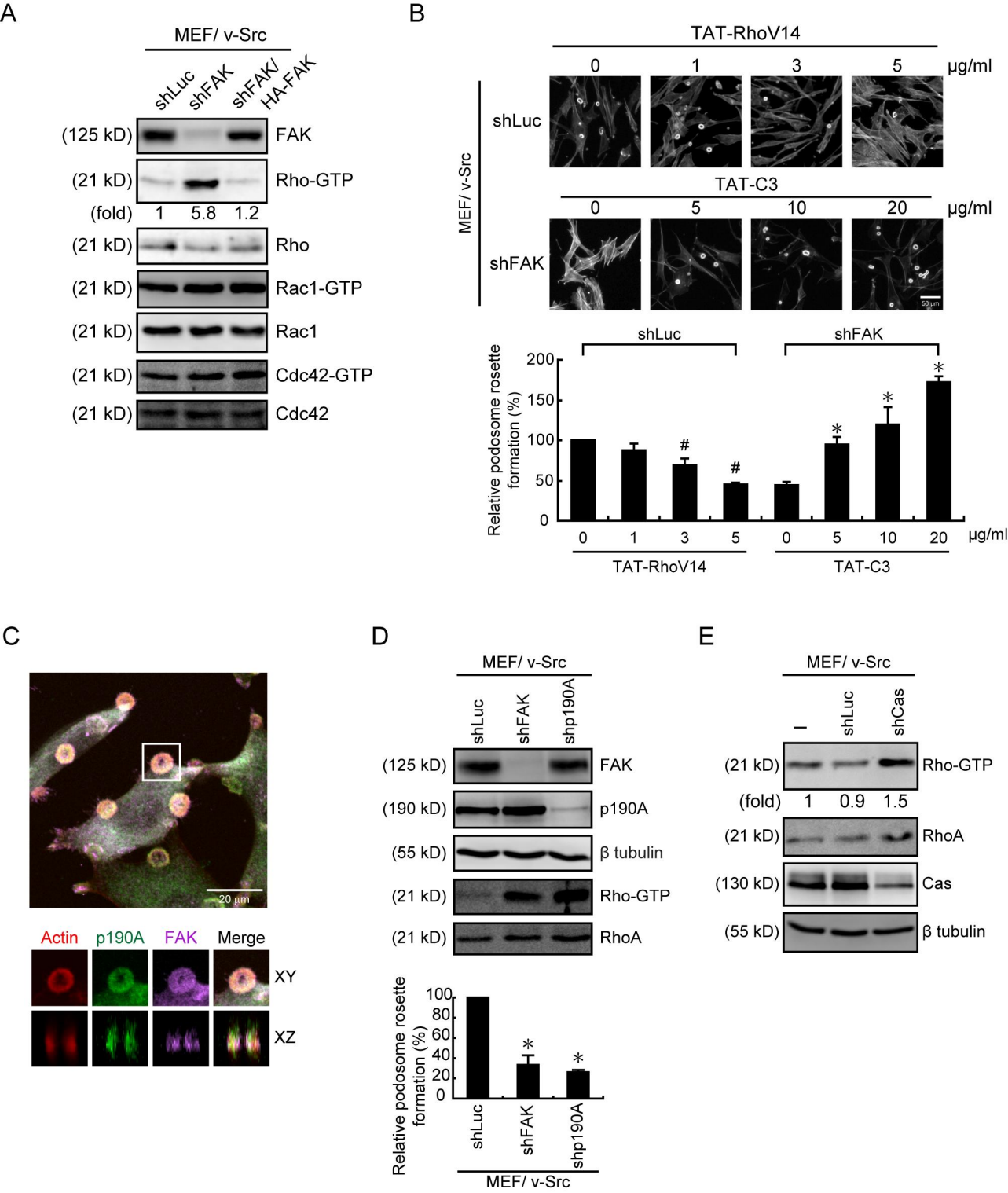
A
MEF/ v-Src
shLuc
shFAK
shFAK/ HA-FAK
(125 kD)
FAK
(21 kD)
Rho-GTP
(fold) 1 5.8 1.2
(21 kD)
Rho
(21 kD)
Rac1-GTP
(21 kD)
Rac1
(21 kD)
Cdc42-GTP
(21 kD)
Cdc42
B
TAT-RhoV14
0 1 3 5 μg/ml
MEF/ v-Src
shLuc
TAT-C3
0 5 10 20 μg/ml
shFAK
50 μm
shLuc
shFAK
Relative podosome rosette formation (%)
200
150
100
50
0
#
#
*
*
*
0 1 3 5 0 5 10 20 μg/ml
TAT-RhoV14
TAT-C3
C
20 μm
Actin
p190A
FAK
Merge
XY
XZ
D
MEF/ v-Src
shLuc
shFAK
shp190A
(125 kD)
FAK
(190 kD)
p190A
(55 kD)
β tubulin
(21 kD)
Rho-GTP
(21 kD)
RhoA
Relative podosome rosette formation (%)
100
80
60
40
20
0
*
*
shLuc
shFAK
shp190A
MEF/ v-Src
E
MEF/ v-Src
–
shLuc
shCas
(21 kD)
Rho-GTP
(fold) 1 0.9 1.5
(21 kD)
RhoA
(130 kD)
Cas
(55 kD)
β tubulin

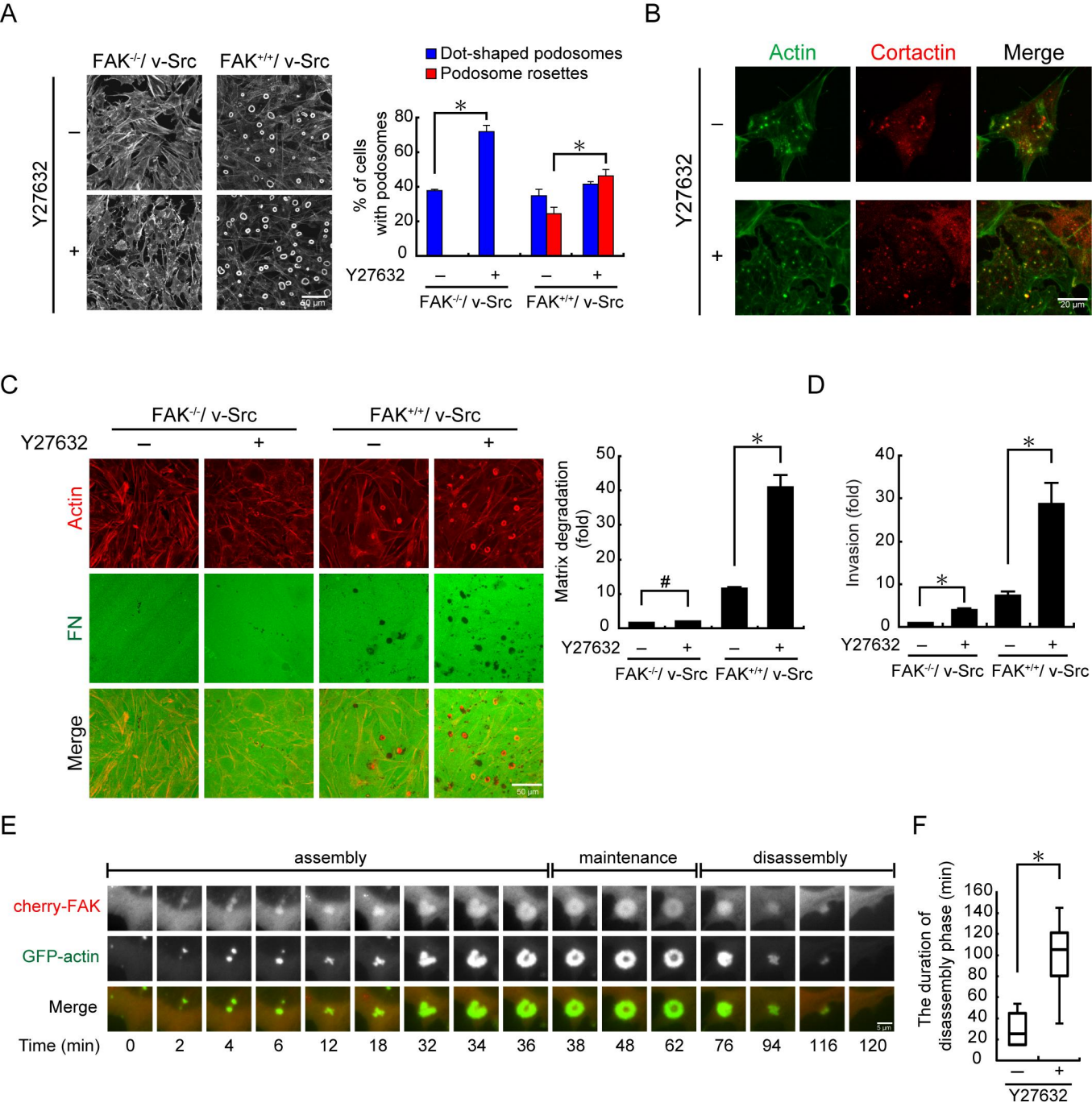
A
FAK-/-/ v-Src
FAK+/+/ v-Src
Y27632
–
+
90 μm
Dot-shaped podosomes
Podosome rosettes
% of cells with podosomes
80
60
40
20
0
*
*
Y27632
–
+
–
+
FAK-/-/ v-Src
FAK+/+/ v-Src
B
Actin
Cortactin
Merge
Y27632
–
+
20 μm
C
FAK-/-/ v-Src
FAK+/+/ v-Src
Y27632
–
+
–
+
Actin
FN
Merge
50 μm
Matrix degradation (fold)
50
40
30
20
10
0
#
*
Y27632
–
+
–
+
FAK-/-/ v-Src
FAK+/+/ v-Src
D
Invasion (fold)
40
30
20
10
0
*
*
Y27632
–
+
–
+
FAK-/-/ v-Src
FAK+/+/ v-Src
E
assembly
maintenance
disassembly
cherry-FAK
GFP-actin
Merge
5 μm
Time (min)
0
2
4
6
12
18
32
34
36
38
48
62
76
94
116
120
F
The duration of disassembly phase (min)
160
140
120
100
80
60
40
20
0
*
–
+
Y27632

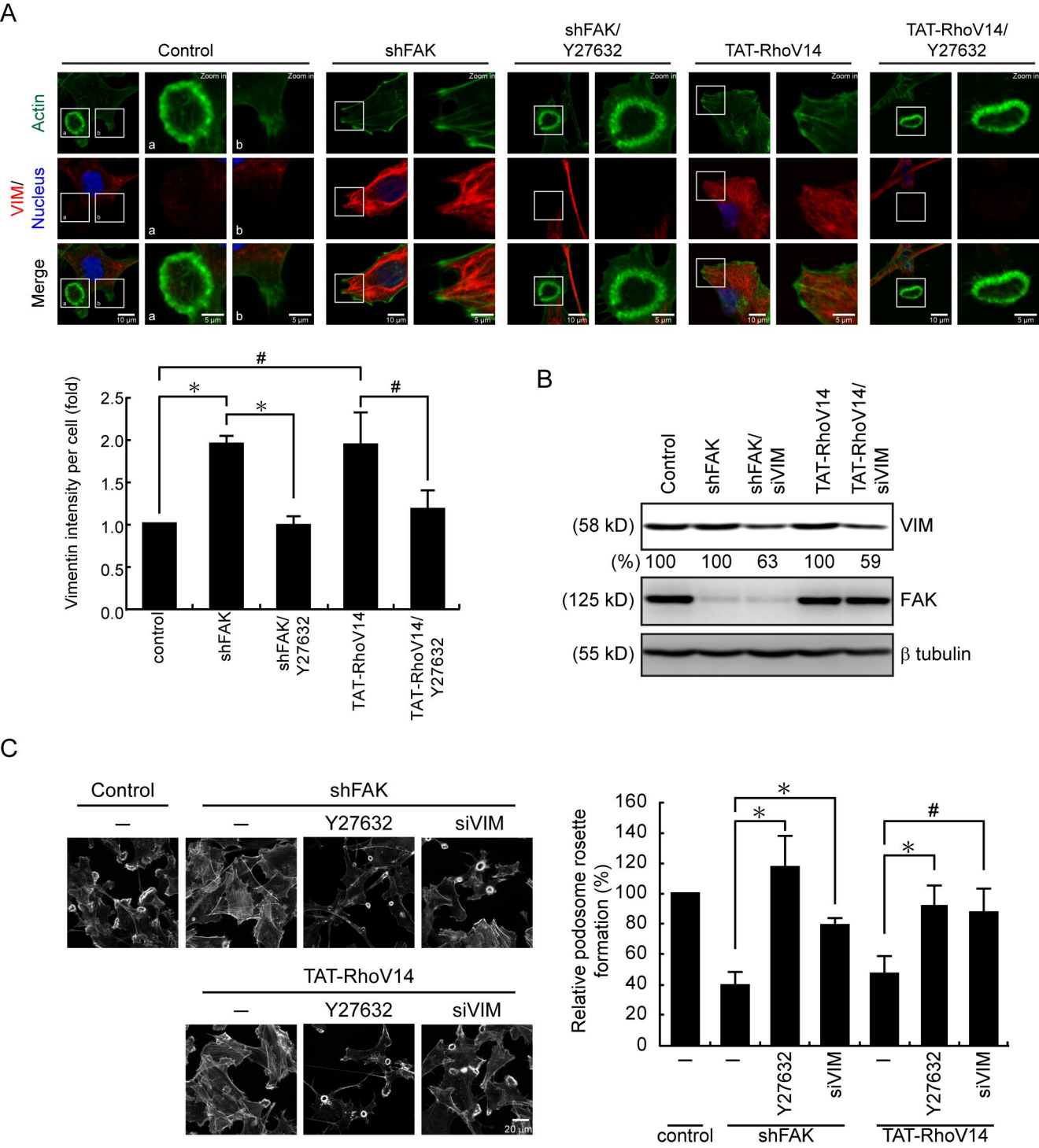
A
Control
shFAK
shFAK/
Y27632
TAT-RhoV14
TAT-RhoV14/
Y27632
Actin
VIM/
Nucleus
Merge
Zoom in
a
b
10 μm
5 μm
Vimentin intensity per cell (fold)
2.5
2.0
1.5
1.0
0.5
0.0
*
*
#
#
control
shFAK
shFAK/
Y27632
TAT-RhoV14
TAT-RhoV14/
Y27632
B
Control
shFAK
shFAK/
siVIM
TAT-RhoV14
TAT-RhoV14/
siVIM
(58 kD)
VIM
(%) 100 100 63 100 59
(125 kD)
FAK
(55 kD)
β tubulin
C
Control
shFAK
–
Y27632
siVIM
TAT-RhoV14
20 μm
Relative podosome rosette formation (%)
160
140
120
100
80
60
40
20
0
*
*
*
#
–
Y27632
siVIM
control
shFAK
TAT-RhoV14

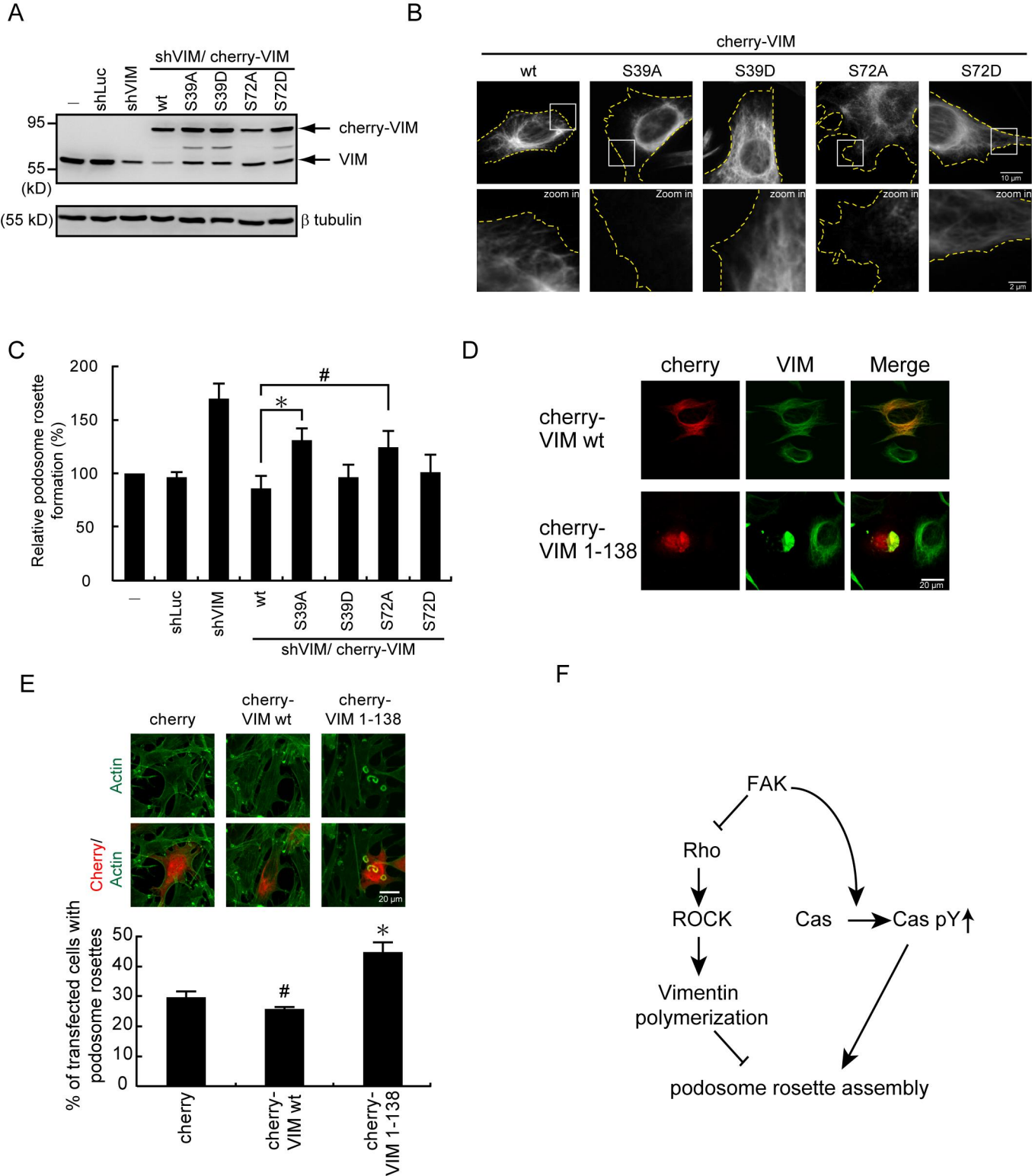
A
shVIM/ cherry-VIM
–
shLuc
shVIM
wt
S39A
S39D
S72A
S72D
95
55
(kD)
cherry-VIM
VIM
(55 kD)
β tubulin
B
cherry-VIM
wt
S39A
S39D
S72A
S72D
zoom in
10 μm
2 μm
C
Relative podosome rosette formation (%)
200
150
100
50
0
#
*
shVIM/ cherry-VIM
D
cherry
VIM
Merge
cherry-VIM wt
cherry-VIM 1-138
20 μm
E
cherry
cherry-VIM wt
cherry-VIM 1-138
Actin
Cherry/ Actin
20 μm
% of transfected cells with podosome rosettes
50
40
30
20
10
0
#
*
F
FAK
Rho
ROCK
Cas
Cas pY
Vimentin polymerization
podosome rosette assembly

A

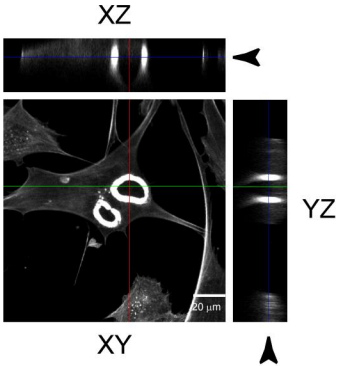

B

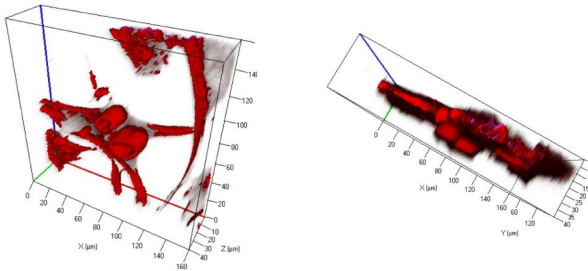

C

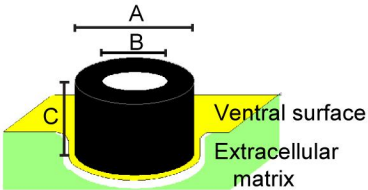

A: 15.2 ± 4.8 µm
B: 6.8 ± 3.8 µm
C: 18.0 ± 6.2 µm

D

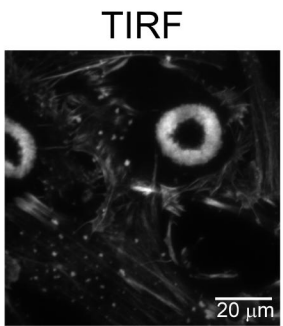

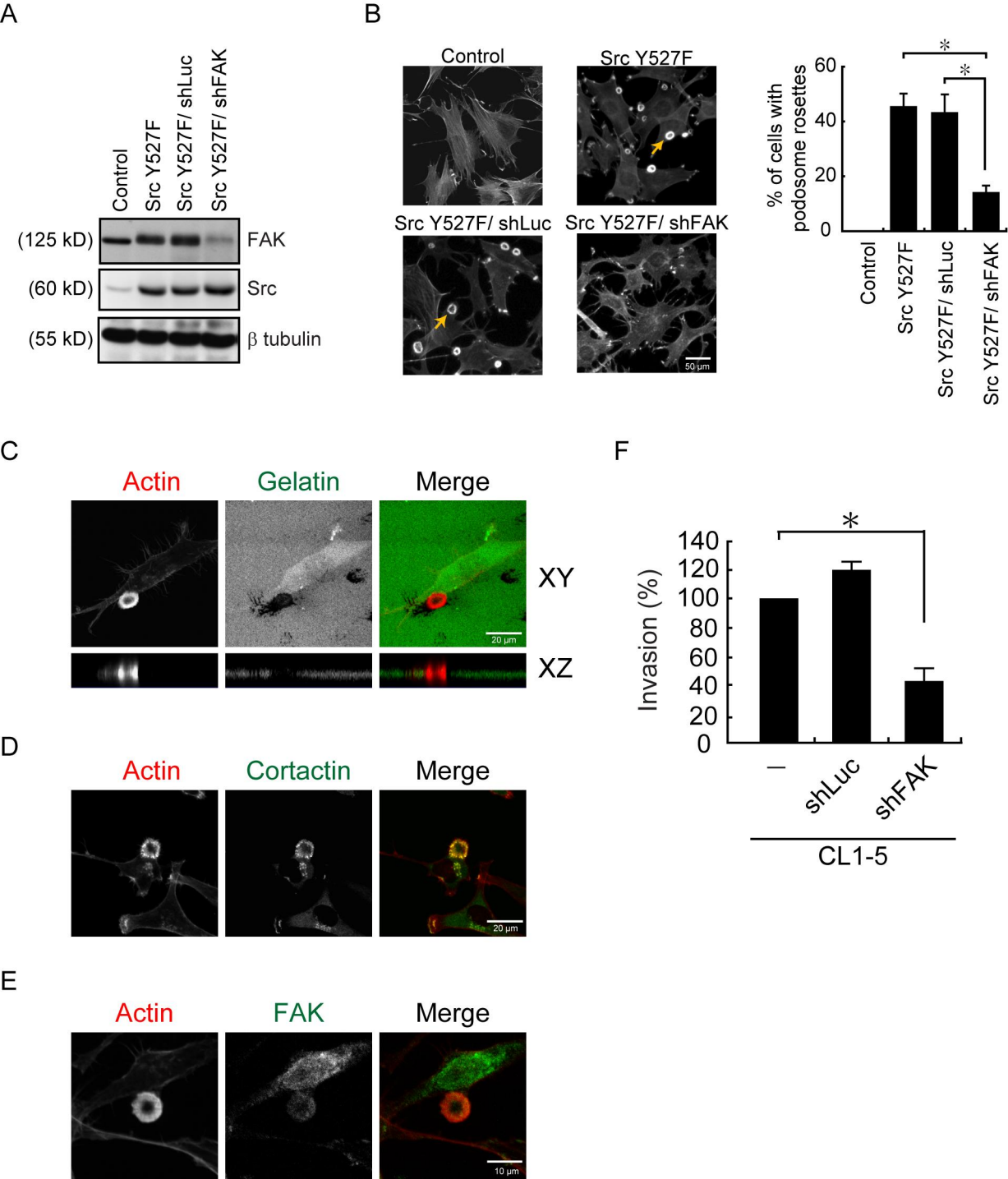
A
Control
Src Y527F
Src Y527F/ shLuc
Src Y527F/ shFAK
(125 kD)
FAK
(60 kD)
Src
(55 kD)
β tubulin
B
Control
Src Y527F
Src Y527F/ shLuc
Src Y527F/ shFAK
50 μm
% of cells with podosome rosettes
60
40
20
0
*
*
Control
Src Y527F
Src Y527F/ shLuc
Src Y527F/ shFAK
C
Actin
Gelatin
Merge
XY
XZ
20 μm
D
Actin
Cortactin
Merge
20 μm
E
Actin
FAK
Merge
10 μm
F
Invasion (%)
140
120
100
80
60
40
20
0
*
–
shLuc
shFAK
CL1-5

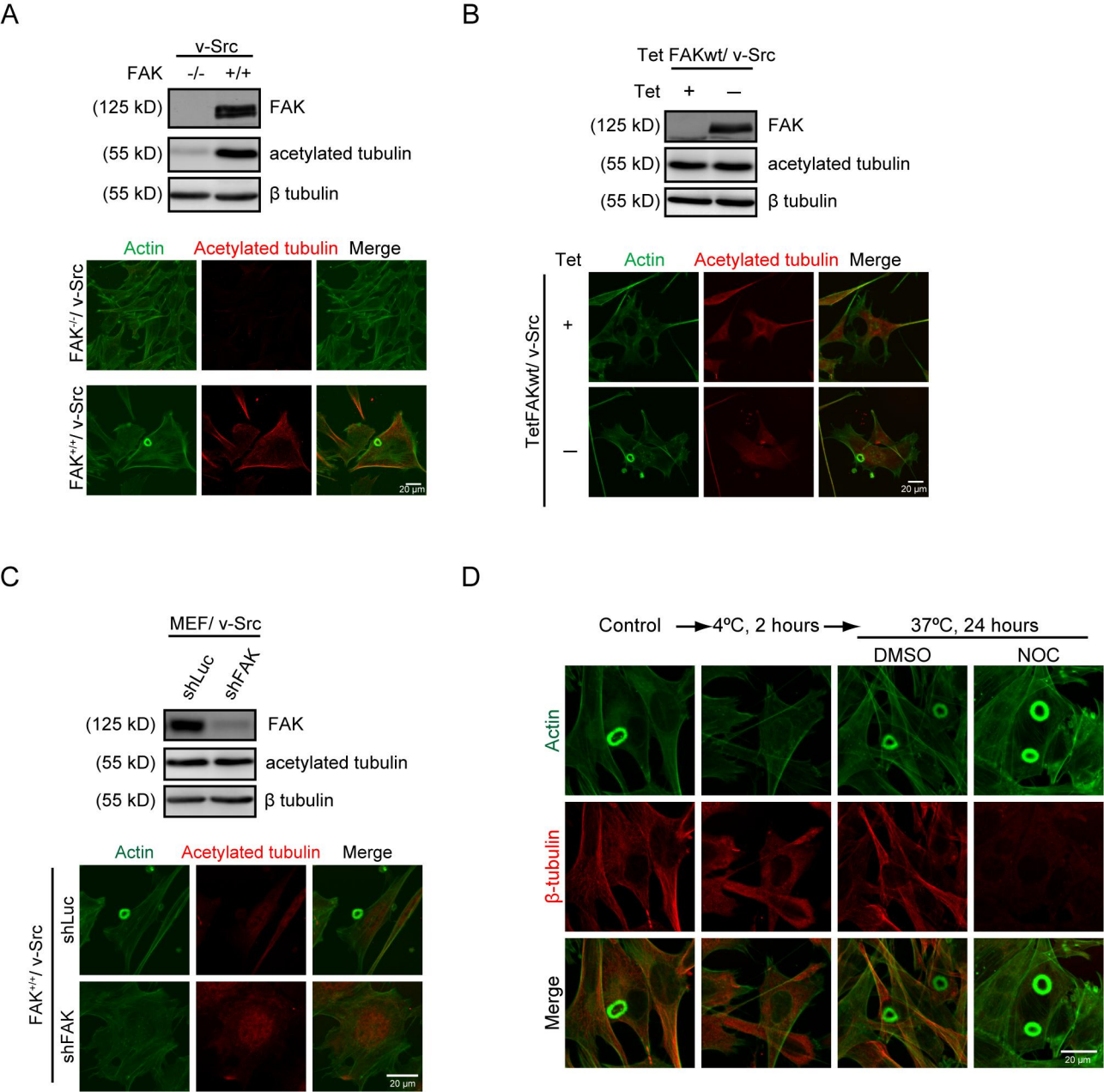
A
v-Src
FAK -/- +/+
(125 kD) FAK
(55 kD) acetylated tubulin
(55 kD) β tubulin
Actin
Acetylated tubulin
Merge
FAK+/+/ v-Src
FAK+/+/ v-Src
20 μm
B
Tet FAKwt/ v-Src
Tet + —
(125 kD) FAK
(55 kD) acetylated tubulin
(55 kD) β tubulin
Tet
Actin
Acetylated tubulin
Merge
TetFAKwt/ v-Src
+
—
20 μm
C
MEF/ v-Src
shLuc
shFAK
(125 kD) FAK
(55 kD) acetylated tubulin
(55 kD) β tubulin
Actin
Acetylated tubulin
Merge
FAK+/+/ v-Src
shLuc
shFAK
20 μm
D
Control
4ºC, 2 hours
37ºC, 24 hours
DMSO
NOC
Actin
β-tubulin
Merge
20 μm

A

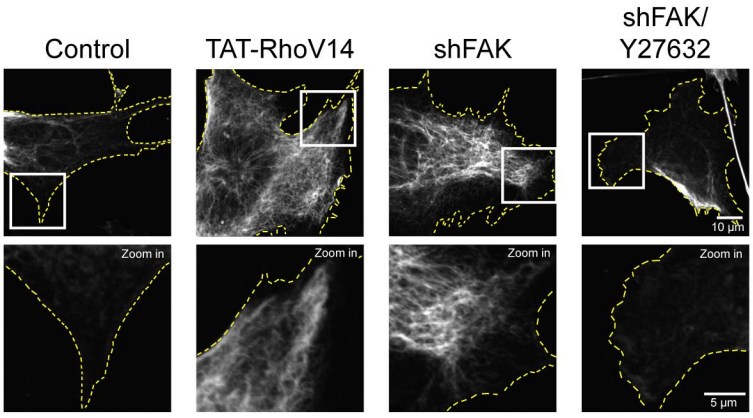
Control
TAT-RhoV14
shFAK
shFAK/
Y27632
Zoom in
Zoom in
Zoom in
Zoom in
10 μm
5 μm

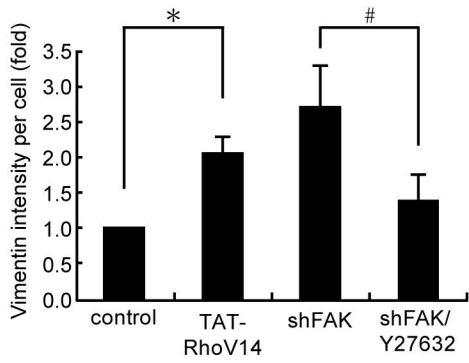
Vimentin intensity per cell (fold)
3.5
3.0
2.5
2.0
1.5
1.0
0.5
0.0
*
#
control
TAT-
RhoV14
shFAK
shFAK/
Y27632

B

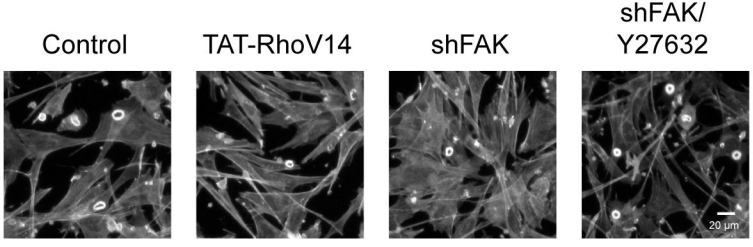
Control
TAT-RhoV14
shFAK
shFAK/
Y27632
20 μm

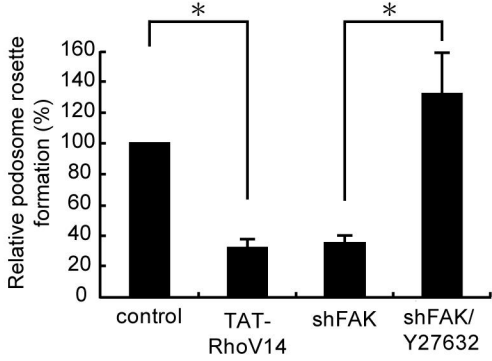
Relative podosome rosette
formation (%)
160
140
120
100
80
60
40
20
0
*
*
control
TAT-
RhoV14
shFAK
shFAK/
Y27632